On Identification of Well-Conditioned Nonlinear Systems: Application to Economic Model Predictive Control of Nonlinear Processes

Anas Alanqar and Helen Durand
Dept. of Chemical and Biomolecular Engineering, University of California, Los Angeles, CA 90095

Panagiotis D. Christofides
Dept. of Chemical and Biomolecular Engineering, University of California, Los Angeles, CA 90095

Dept. of Electrical Engineering, University of California, Los Angeles, CA 90095

DOI 10.1002/aic.14942
Published online July 24, 2015 in Wiley Online Library (wileyonlinelibrary.com)

The focus of this work is on economic model predictive control (EMPC) that utilizes well-conditioned polynomial nonlinear state-space (PNLSS) models for processes with nonlinear dynamics. Specifically, the article initially addresses the development of a nonlinear system identification technique for a broad class of nonlinear processes which leads to the construction of PNLSS dynamic models which are well-conditioned over a broad region of process operation in the sense that they can be correctly integrated in real-time using explicit numerical integration methods via time steps that are significantly larger than the ones required by nonlinear state-space models identified via existing techniques. Working within the framework of PNLSS models, additional constraints are imposed in the identification procedure to ensure well-conditioning of the identified nonlinear dynamic models. This development is key because it enables the design of Lyapunov-based EMPC (LEMPC) systems for nonlinear processes using the well-conditioned nonlinear models that can be readily implemented in real-time as the computational burden required to compute the control actions within the process sampling period is reduced. A stability analysis for this LEMPC design is provided that guarantees closed-loop stability of a process under certain conditions when an LEMPC based on a nonlinear empirical model is used. Finally, a classical chemical reactor example demonstrates both the system identification and LEMPC design techniques, and the significant advantages in terms of computation time reduction in LEMPC calculations when using the nonlinear empirical model. © 2015 American Institute of Chemical Engineers *AIChE J*, 61: 3353–3373, 2015
Keywords: economic model predictive control, nonlinear system identification, numerical stability, process control, process optimization, process economics, chemical processes

Introduction

The increasingly competitive and continuously changing world economy has made it necessary to exploit the economic potential of chemical and petrochemical processes which has led engineers to economically optimize process operation to provide long-term economic growth while meeting safety and environmental constraints. One approach for increasing the profitability of industrial processes is to incorporate directly process economic considerations into the feedback control policy. A fairly recent control methodology designed for this purpose is economic model predictive control (EMPC). Specifically, EMPC employs an optimization problem incorporating dynamic economic considerations in its cost function and constraints to operate the process in a time-varying manner to optimize process economics.[1–3] A number of works have shown the potential of this economic optimization-based feedback control strategy to improve profitability of chemical processes. For example, certain nominal formulations of EMPC have been proven to perform at least as well in infinite-time as operating at the optimal steady-state,[1] and finite-time optimality has also been examined and demonstrated for EMPC without terminal constraints or terminal cost in Ref. 4. Furthermore, both finite-time and infinite-time performance have been characterized in Ref. 5 for a two-layer EMPC formulated with performance constraints. In addition to EMPC performance, a variety of other topics have been addressed for EMPC, such as stability[6–8] and computation time reduction[9–11] (see also the review paper[12] and the references therein for additional works on EMPC).

The primary assumption in using any type of model predictive control (MPC) is the availability of a process model that is utilized to predict future values of the process states. Constructing a process model is done either through first principles or via system identification. First-principles models attempt to capture the essential physicochemical mechanisms and phenomena and are derived from an understanding of the

Correspondence concerning this article should be addressed to P. D. Christofides at pdc@seas.ucla.edu

mathematics and science that can be used to describe a given process. It can thus be very difficult to derive a first-principles model if a process is complex or poorly understood. A significant amount of research has been performed throughout the last three decades to develop system identification methods that exploit input/output process data to arrive at linear or nonlinear empirical models.[13–20] Process control engineers routinely use system identification techniques to obtain input/output empirical models or state-space empirical models.

More specifically, a variety of input/output system identification methods (e.g., (nonlinear) autoregressive moving average with exogenous input ((N)ARMAX) methods, or methods that identify polynomial and neural-network models[16,17,21]) have been developed. Input/output models, such as Hammerstein models,[19] Wiener models,[22,23] Hammerstein-Wiener models,[24] polynomial ARX models,[20,25] and neural Wiener models[26–28] have been used in tracking MPC applications (where the control objective is to regulate a process at a potentially optimal steady-state).

Another type of empirical modeling that is also widely used is empirical state-space modeling. System identification techniques have been developed to identify linear and nonlinear state-space models. Several linear state-space system identification methods based on input/output data, such as optimization-based methods and subspace model identification, have been developed that can be used for multiple-input/multiple-output (MIMO) systems because of their ability to model interactions among process states.[13–15,29–34] Subspace model identification has been investigated for use in MPC[35] and can be carried out through a variety of techniques such as the canonical variate algorithm (CVA),[14] the multivariable output error state-space algorithm (MOESP),[13,31,32,36] and numerical algorithms for subspace state-space system identification (N4SID).[15] Grey box nonlinear state-space system identification methods include maximum likelihood parameter estimation methods[37] and optimization-based methods.[38]

In both input/output and state-space empirical modeling, a wide variety of polynomial functions have been used to identify nonlinear models. Polynomial functions used in input/output system identification include Chebyshev polynomials,[39] Volterra polynomials,[17,40] polynomial ARX models,[20] Laguerre polynomials,[41] and polynomial neural networks.[17] Traditional empirical modeling approaches focus on a certain class of nonlinear systems like Wiener-Hammerstein or neural networks but nonlinear state-space models cover a much larger class of systems. The need for a general nonlinear system identification technique that can represent many classes of nonlinear systems led to the development of state-space nonlinear system identification techniques based on input/output data. The polynomial nonlinear state-space (PNLSS) approach is a system identification method for MIMO systems that leads to a model of a multivariable nonlinear system based purely on input/output data.[18,42–46] PNLSS is a promising all-purpose nonlinear system identification method that can be used for many different types of systems, including those that are described by bilinear models, Wiener-Hammerstein models, and models with nonlinearities appearing in the states or inputs, or appearing in both.[18,42,45,46]

In the PNLSS approach, a linear state-space model is first obtained and it is then extended to a nonlinear model for the system using polynomial nonlinear terms with coefficients identified through an optimization problem.[18,42–46] The linear part can be obtained using the best linear fit or least-squares, or using subspace system identification.[18,42,45,46] The linear model is determined first so that the nonlinear model subsequently identified will achieve a performance at least as good as that of the linear model in a small neighborhood of the measured process states used in the identification process.[18] PNLSS has shown superior results over linear models in various applications including control and modeling applications[43,45] and identifying the dynamics of electrical circuits.[47] The use of PNLSS in nonlinear model predictive control (NMPC) for an automotive clutch system has also been presented.[44] A crucial advantage of PNLSS is that it is very straightforward to apply for multivariable systems and has a very significant computation time benefit for low-order polynomials (e.g., polynomial models with orders two or three).[18,46] A potential disadvantage of PNLSS is that it may lead to ill-conditioned models which may need a very small time step to be solved correctly with explicit numerical integration methods.

Motivated by the above, this work initially develops a nonlinear system identification technique for a broad class of nonlinear processes which leads to the construction of PNLSS dynamic models which are well-conditioned over a broad region of process operation. This technique takes advantage of the framework of PNLSS models and utilizes additional constraints on the stiffness ratio of the Jacobian of the nonlinear identified models at various points in the region of process operation to ensure that the resulting models can be solved without using an unnecessarily small time step of integration when explicit temporal-integration methods are used. Subsequently, the design of Lyapunov-based economic model predictive control (LEMPC) systems for nonlinear processes using the well-conditioned nonlinear models is addressed and sufficient conditions are derived for closed-loop stability. Throughout the article, a classical chemical process example is used to illustrate the application and point out the advantages of the proposed system identification and LEMPC design techniques.

Preliminaries

Notation

The operator $|\cdot|$ is used to denote the vector Euclidean norm, the operator $|\cdot|_p$ is used to denote the vector p-norm, and the operator $||\cdot||$ is used to denote any matrix norm. The transpose of a vector x is represented by the symbol x^T. The symbol Ω_ρ denotes a level set of a continuously differentiable, positive definite scalar-valued function $V(x)$ ($\Omega_\rho := \{x \in R^n : V(x) \leq \rho\}$).

Class of systems

In this work, the class of systems to be considered are nonlinear, continuous-time systems with affine inputs, with dynamics described according to the system of differential equations

$$\dot{x}(t) = f_p(x(t), w(t)) + \tilde{G}(x(t), w(t))u(t) \tag{1}$$

where the state vector is $x \in R^n$, the input vector is $u \in R^m$, the disturbance vector is $w \in R^l$, $f_p(x(t), w(t)) : R^n \times R^l \rightarrow R^n$ is a vector function, and $\tilde{G}(x(t), w(t)) : R^n \times R^l \rightarrow R^n \times R^m$ is a matrix of functions of x and w. It is assumed that the component functions of f_p and $\tilde{G}$ are analytic on $R^n \times R^l$ such that they are infinitely differentiable and locally expressed with a convergent power series.

We also assume that since all control actuators u have physical limits, the control actions are bounded within a convex set $U := \{u \in R^m : u_i^{\min} \leq u_i \leq u_i^{\max},\ i = 1,\ \ldots,\ m\}$. In addition, all disturbances to the system are assumed to have a known bound of $\theta > 0$ (for all t, $|w(t)| \leq \theta$). The origin is assumed to be an equilibrium point of Eq. 1 ($f_p(0,0) = 0$ when $u = 0$).

Only nonlinear systems for which an explicit controller exists that can make the origin of Eq. 1 locally exponentially stable in the absence of disturbances ($w(t) \equiv 0$), while meeting the constraints on the control actions, will be considered. When such an explicit controller $h(x) \in U$ exists, converse Lyapunov theorems state that a positive definite, continuously differentiable, scalar-valued function $V(x)$ and positive constants c_1, c_2, c_3, and c_4 exist that result in the following inequalities[48,49]

$$c_1|x|^2 \leq V(x) \leq c_2|x|^2 \tag{2a}$$

$$\frac{\partial V(x)}{\partial x}\left(f_p(x,0)+\tilde{G}(x,0)h(x)\right) \leq -c_3|x|^2 \tag{2b}$$

$$\left|\frac{\partial V(x)}{\partial x}\right| \leq c_4|x| \tag{2c}$$

for any x within the open connected set $D \subseteq R^n$ that includes the origin. Methods for developing $h(x)$ are available for various classes of systems (see, for example, Ref. 50–53). The stability region Ω_ρ for the closed-loop system of Eq. 1 under the controller $h(x)$ is defined as a level set of V (a set within which $V(x) \leq \rho$) within D where $\dot{V}$ is negative.

System Identification

In this work, we use the PNLSS approach to obtain a model that is nonlinear in the states and affine in the inputs, with the following form

$$\frac{dx}{dt} = \underbrace{Ax+P_z(x)}_{=:f(x)} + Bu \tag{3}$$

where $x \in R^n$ and $u \in R^m$ are the state vector and the input vector respectively, A is a constant square matrix of dimension n, and $B \in R^{n\times m}$ is a constant matrix. The notation $P_z(x)$ denotes a nonlinear vector function that includes polynomial terms of order two and higher, with the subscript z used to indicate that the polynomial is a z^{th}-order polynomial. $P_z(x)$ is defined by the following equations

$$P_z(x) = E\xi(x) \tag{4a}$$

$$\xi(x) = [x_1^2 \quad x_1x_2 \ \ldots \quad x_n^z]^T \tag{4b}$$

where the vector $\xi(x)$ contains nonlinear monomials in x of order two and higher up to a chosen order z, and the constant matrix E contains the coefficients multiplying the nonlinear monomials in $\xi(x)$. The order z of the polynomial is chosen before data are fit to the model of Eq. 3. As an example, when $n = 2$ and $z = 3$, $\xi(x)$ has the following form

$$\xi(x) = [x_1^2 \quad x_1x_2 \quad x_2^2 \quad x_1^3 \quad x_1^2x_2 \quad x_1x_2^2 \quad x_2^3]^T \tag{5}$$

PNLSS system identification methodology

The PNLSS identification problem is to find the terms A, B, and E in Eqs. 3–4 when the only available information is process input/output data.[18,42–46] For the case when all states are available as measured outputs (full state feedback), an optimization problem can be used to find these terms that involves the following two steps:

1. A linear state-space model is obtained using a frequency domain subspace identification algorithm.

2. The linear model is used as an initial guess for a nonlinear optimization problem to identify a nonlinear model that captures the nonlinear behavior of the system.

To simplify the presentation in this work, we will consider that full state feedback is available and thus the measurements of the states can be used directly in order to obtain the PNLSS model. To implement the PNLSS method, one obtains $Z + 1$ state measurements of the system ($x_m(v)$, $v = 0, ..., Z$, where $x_m(v)$ is the vector of measured states in deviation variable form at time $\tilde{t}_v = v\tilde{\Delta}$ and $\tilde{\Delta}$ is the time between measurements) with a known sequence of inputs. Then, using the same initial state $x_m(0)$ and the same sequence of inputs, Z modeled states (denoted as $x(v)$, $v = 1, ..., Z$, where $x(v)$ is the vector of modeled states in deviation variable form at time $\tilde{t}_v = v\tilde{\Delta}$) are obtained via numerical integration of the model to be identified (Eq. 3). The goal is then to minimize the difference between the measured and modeled states that correspond to the same times in the simulation by adjusting the model parameters A, B, and E in Eq. 3.

We denote the vector of measured states (in deviation form) that will be used in the PNLSS objective function in a vector form (the problem could be reformulated with the states in a matrix form if desired) as

$$x_m = [x_m^T(1) \ \ x_m^T(2) \ \ \ldots \ \ x_m^T(Z)]^T \tag{6}$$

and the modeled states as

$$x_p = [x^T(1) \ \ x^T(2) \ \ \ldots \ \ x^T(Z)]^T \tag{7}$$

where $x_m(0) = x(0)$ is the initial state ($x_m(0) = x(0) = 0$ if we start from the steady-state). Using this notation, the PNLSS model is identified via a nonlinear optimization problem formulated as

$$\min_{\eta} \quad \Phi(x_m - x_p) \tag{8a}$$

$$\text{s.t.} \quad \dot{x} = Ax+P_z(x)+Bu \tag{8b}$$

where η signifies the optimization variables A, B, and E and Φ is a positive definite cost function to be minimized. Examples of commonly used functions include the vector 1-norm, vector 2-norm (also called least-squares), weighted least-squares, and a linear combination and/or a product of such functions (the induced matrix 1-norm, induced matrix 2-norm, or combinations/products of these norms are possible cost functions if this is reformulated for the matrix case).

If it is desired to identify a nonlinear model that minimizes the vector p-norm, the optimization problem is reduced to the following nonlinear optimization problem

$$\min_{\eta} \quad |(x_m - x_p)|_p \tag{9a}$$

$$\text{s.t.} \quad \dot{x} = Ax+P_z(x)+Bu \tag{9b}$$

After obtaining the model, this model is validated over a wide range of input/state data. However, the usefulness of the model depends on the purpose it serves. From a NMPC point of view, empirical models need to be well-conditioned so that they can be accurately solved with explicit integration schemes without employing very small time steps to predict

the behavior of the nonlinear system in real-time. Numerical stability of an empirical model is not a central issue when performing linear system identification since the analytic solution of a linear system can be obtained. On the other hand, there is no general method for obtaining the analytic solution of highly coupled nonlinear ordinary differential equations and the numerical integration accuracy is sensitive to the numerical stability of the identified nonlinear model. The system identification procedure does not guarantee that a well-conditioned model will be obtained, so the identified model may be ill-conditioned requiring a very small numerical integration step size to be used.

Remark 1. *The existence of a numerical solution within the accuracy of the numerical integration method used is of concern when using explicit numerical integration methods (e.g., Explicit Euler or Runge-Kutta) as opposed to implicit numerical methods, especially for ill-conditioned nonlinear differential equations. This is because implicit methods are numerically stable for any integration step size, such that only the accuracy of the solution obtained depends on the step size, whereas explicit numerical methods are numerically stable only if the integration step size is sufficiently small, and the threshold at which a step size is sufficiently small is not generally possible to predict for a given system. Despite the relative time step advantage of using implicit methods for numerical integration over explicit ones, implicit methods are very complex to include in system identification and when modeling the outputs and states. Also, implicit methods are computationally expensive and from a predictive control point of view, it is preferred to use explicit methods with a suitable integration step size because they are easier to implement. This preference for explicit methods is demonstrated in much of the theoretical and practical work in MPC through the frequent use of discrete-time models for MPC design and implementation where the state in the next sampling time is determined by states and inputs of the past sampling times, a characteristic of the discrete-time models obtained from the temporal discretization of differential equation models with explicit numerical integration schemes.*

Remark 2. *It was noted that the modeled states x(v), v* $= 1, ..., Z$ *come from the numerical integration of* Eq. 3. *The numerical integration can be performed several different ways in system identification. One method is to perform numerical integration of the model of* Eq. 3 *as is typically done when integrating a differential equation with a given initial condition, and integrating the model between* $\tilde{t}_0$ *and* $\tilde{t}_Z$ *using only the initial state* $x_m(0)$ *and the known input sequence. This complete integration between the initial and final times makes the optimization substantially more burdensome and involved. Another numerical integration method used in practical implementation of system identification methods that is less computationally intensive involves using all of the measured states in the numerical integration used in modeling the states.*[30] *In this method, each measurement is used as an initial condition for numerical integration of* Eq. 3 *to obtain only the following modeled state (i.e., to obtain the value of x(v),* $v = 1, ..., Z$, *numerical integration over only one time interval* $\tilde{\Delta}$ *is performed with the initial condition for each x(v) as* $x_m(v-1)$, $v = 1, ..., Z$). *As the number of measured states increases, the number of numerical integration steps between* $x_m(v-1)$ *and x(v) decreases. When the same number of measurements are used as the number of modeled states such that only one integration step is needed for each x(v), the optimization problem is much easier to solve as will be demonstrated in the example.*

Table 1. CSTR Parameters

$F = 5.0$	$\frac{m^3}{h}$	$k_0 = 8.46\times10^6$	$\frac{m^3}{kmol\ h}$
$T_0 = 300$	K	$\Delta H = -1.15\times10^4$	$\frac{kJ}{kmol}$
$V = 1.0$	m^3	$E = 5.0\times10^4$	$\frac{kJ}{kmol}$
$C_p = 0.231$	$\frac{kJ}{kg\ K}$	$\rho_L = 1000$	$\frac{kg}{m^3}$
$R = 8.314$	$\frac{kJ}{kmol\ K}$		

Motivating example: PNLSS application to a chemical process example

To illustrate the importance of considering model well-conditioning when deriving an empirical model for a process, a chemical process example is presented in this section.

Specifically, a second-order irreversible reaction that forms the product B from the reactant A occurs in a non-isothermal, well-mixed continuously stirred tank reactor (CSTR). The CSTR is fed by an inlet stream containing A with molar concentration C_{A0} in an inert solvent at a feed volumetric flow rate F and feed temperature T_0. The reaction is exothermic, and the CSTR is operated non-isothermally with heat supplied/removed at heat rate Q. The liquid in the CSTR is assumed to have constant heat capacity C_p and constant liquid density ρ_L, and to be maintained at a constant volume V. The dynamic model equations for the CSTR are developed from standard mass and energy balances and have the form

$$\frac{dC_A}{dt} = \frac{F}{V}(C_{A0} - C_A) - k_0 e^{-E/RT} C_A^2 \tag{10a}$$

$$\frac{dT}{dt} = \frac{F}{V}(T_0 - T) - \frac{\Delta H k_0}{\rho_L C_p} e^{-E/RT} C_A^2 + \frac{Q}{\rho_L C_p V} \tag{10b}$$

where C_A is the concentration of the reactant A inside the reactor and T is the reactor temperature. The reaction kinetics are modeled using the Arrhenius equation, with pre-exponential factor k_0, activation energy E, and enthalpy of reaction ΔH (see Table 1 for the values of the reactor parameters). The CSTR is operated at the steady-state $[C_{As}\ T_s] = [1.2\ \text{kmol/m}^3\ 438.0\ \text{K}]$, which is open-loop asymptotically stable and corresponds to a steady-state inlet concentration of $C_{A0s} = 4.0\ \text{kmol/m}^3$ and a heat rate of $Q_s = 0.0\ \text{kJ/h}$.

The dynamic model of Eq. 10 is of the following form (using the notation of Eq. 1)

$$\dot{x}(t) = f_p(x(t), 0) + \tilde{G}(x(t), 0)u(t) \tag{11}$$

where the vectors of states and inputs in Eq. 11 are defined in deviation form as

$$x = [x_1\ x_2]^T = [C_A - C_{As}\ T - T_s]^T \tag{12}$$

$$u = [u_1\ u_2]^T = [C_{A0} - C_{A0s}\ Q - Q_s]^T \tag{13}$$

The inlet concentration C_{A0} and the rate Q at which heat is supplied to or removed from the CSTR can be manipulated to affect the reactor state variables. These manipulated inputs are subject to the constraints

$$0.5 \le C_{A0} \le 7.5\ \text{kmol/m}^3 \tag{14a}$$

$$-5.0\times10^5 \le Q \le 5.0\times10^5\ \text{kJ/h} \tag{14b}$$

To show the influence of step size on the integration of an empirical model resulting from system identification of a process with the dynamics of Eq. 10, the PNLSS approach of Eq.

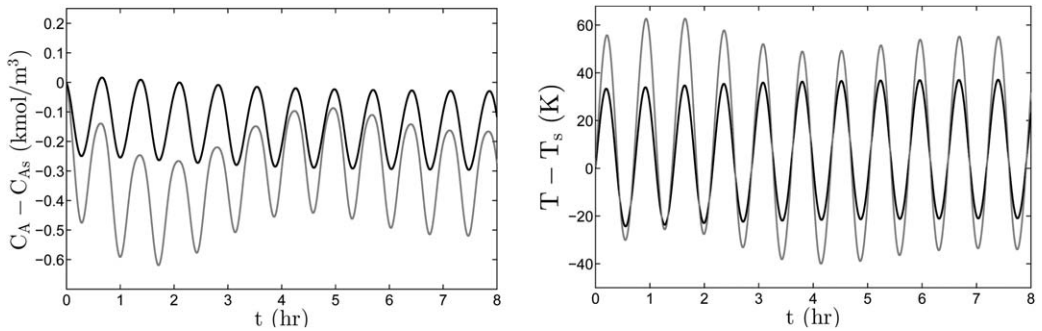

Figure 1. State trajectories of the first-principles CSTR model of Eq. 10 (black trajectory) and the identified PNLSS model of Eq. 15, $h_c = 10^{-4}$ h (gray trajectory) when the heat rate and concentration inputs are varied sinusoidally with amplitudes 55,000 kJ/h and 0.25 kmol/m^3, respectively, and both with frequency 8.72 rad/h.

9 with $p = 2$ was applied to this chemical process. To generate the input/state data necessary to implement the PNLSS method, several steps in the inputs to the CSTR were simulated, and the input/state data was obtained from the integration of the dynamic model of Eq. 10 subject to the input changes. It was determined that the accuracy of the numerical integration of the CSTR model of Eq. 10 was sufficient with the Explicit Euler method using an integration step size of $h_c = 10^{-4}$ h, so this numerical integration procedure and step size were used for the first-principles process model of Eq. 10 throughout this article. From the input/state data, a PNLSS model of the form of Eq. 3, where the vectors of states x and inputs u are as defined in Eqs. 12 and 13, was obtained. All PNLSS optimization problems in this article were solved using the open-source nonlinear interior point optimization solver Ipopt.[54] The states were modeled using both numerical integration methods discussed in Remark 2 (the states were modeled using only the initial state with the sequence of inputs, and also by using all of the measured states and the input sequence) and the resulting empirical models were almost identical. However, solving the system identification optimization problem of Eq. 9 using the second method (using all measured states) was much less computationally intensive than using the first method (using only the initial measured state), so the second method will be used for all PNLSS optimization problems for this chemical process example throughout the rest of the article. The term $P_z(x)$ in Eq. 3 was chosen to be a second-order polynomial so $z = 2$ and $n = 2$. The identified nonlinear continuous-time model of the CSTR is

$$\frac{dx_1}{dt} = -32.64x_1 - 0.479x_2 - 31.2x_1^2 - 1.0016x_1x_2 - 0.0075x_2^2 + 5.53u_1 - 0.000008u_2 \quad (15a)$$

$$\frac{dx_2}{dt} = 1398x_1 + 17.79x_2 - 30x_1^2 + 24.94x_1x_2 + 0.381x_2^2 - 1076u_1 + 0.00476u_2 \quad (15b)$$

This model is very sensitive to the numerical integration step. When the inputs are modeled as sinusoids and the process model is integrated with an integration step of $h_c = 10^{-4}$ h with the Explicit Euler method and the resulting trajectories are compared to those of the first-principles CSTR process model of Eq. 10 using the same input and same step size, there are significant differences in the values of the states x_1 and x_2 between the two models, as shown in Figure 1. However, when those same first-principles CSTR trajectories are compared with the trajectories resulting from using an integration step of $h_c = 10^{-6}$ h in the model of Eq. 15 with the same sinusoidal input, the first-principles and PNLSS trajectories are very close, as shown in Figure 2.

Figure 2 shows good agreement between the state trajectories using the first-principles CSTR model of Eq. 10 and the empirical nonlinear model of Eq. 15 when using the smaller step size. In order to quantify the difference between the two behaviors, the average squared error in the concentration and temperature over eight hours of operation, when a step size $h_c = 10^{-6}$ h is used to integrate the empirical model, is calculated as follows

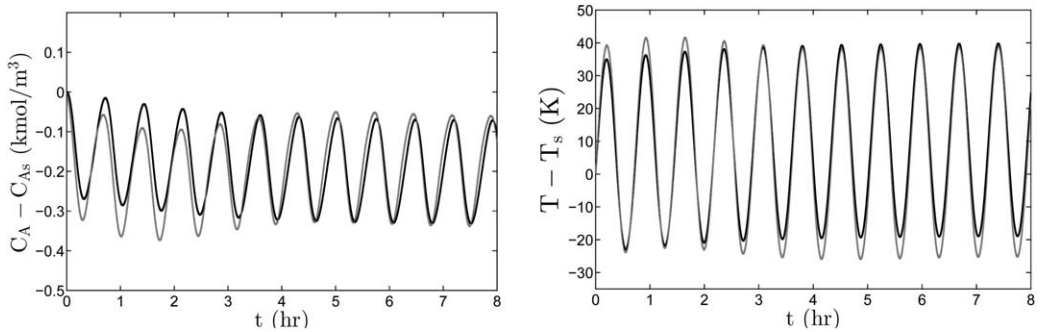

Figure 2. State trajectories of the first-principles CSTR model of Eq. 10 (black trajectory) and the identified PNLSS model of Eq. 15, $h_c = 10^{-6}$ h (gray trajectory) when the heat rate and concentration inputs are varied sinusoidally with amplitudes 55,000 kJ/h and 0.25 kmol/m^3, respectively, and both with frequency 8.72 rad/h.

$$\frac{1}{8}\int_0^8 (x_{1p}(t)-x_{1m}(t))^2\ dt = 1.6821\times10^{-4} \tag{16}$$

$$\frac{1}{8}\int_0^8 (x_{2p}(t)-x_{2m}(t))^2\ dt = 1.3059 \tag{17}$$

where x_{1p} and x_{1m} are the modeled and measured concentrations respectively, and x_{2p} and x_{2m} are the modeled and measured temperatures respectively.

Proposed approach for PNLSS system identification

Motivated by the effect of integration step size on the accuracy of the empirical model from the previous example, additional constraints on the PNLSS optimization are proposed. Adding extra constraints that assure well-conditioning of the nonlinear model is essential for effective control. The modified PNLSS optimization problem with the numerical stability constraints has the general form

$$\min_{\eta\in C} \quad \Phi(x_m-x_p) \tag{18a}$$

$$\text{s.t.} \quad F(\eta) = 0 \tag{18b}$$

$$R(\eta) \le 0 \tag{18c}$$

The optimization variable η represents the parameters A, B, and E of the polynomial nonlinear model of Eqs. 3 and 4. We allow that the values of these parameters belong to the bounded convex set C. $F(\eta)$ and $R(\eta)$ represent equality and inequality constraints that can be used to ensure well-conditioning of the nonlinear identified model. A major cause of ill-conditioning of a system of differential equations is system stiffness, meaning that the dynamics of some states are much faster than the dynamics of others with which they are coupled. As a result, though other numerical stability constraints could be conceived, we will explicitly derive numerical constraints based on stiffness for use in the PNLSS optimization problem.

The stiffness of a system can often be evaluated based on derivative information for the model in the region of operation. For example, the Jacobian of $f(x)$ in Eq. 3 evaluated at s points in the region of operation reveals information about the stiffness of the nonlinear model and its sensitivity to explicit forward numerical integration step sizes. The Jacobian of $f(x)$ evaluated at state-space point j is defined as the matrix of partial derivatives of the component functions f_i with respect to the independent variables x_i, $i = 1, ..., n$

$$J_j = \begin{bmatrix} \frac{\partial f_1}{\partial x_1}|_j & \frac{\partial f_1}{\partial x_2}|_j & \frac{\partial f_1}{\partial x_3}|_j & \cdots & \frac{\partial f_1}{\partial x_n}|_j \\ \frac{\partial f_2}{\partial x_1}|_j & \frac{\partial f_2}{\partial x_2}|_j & \frac{\partial f_2}{\partial x_3}|_j & \cdots & \frac{\partial f_2}{\partial x_n}|_j \\ \cdot & \cdot & \cdot & \cdot & \cdot \\ \cdot & \cdot & \cdot & \cdot & \cdot \\ \cdot & \cdot & \cdot & \cdot & \cdot \\ \frac{\partial f_n}{\partial x_1}|_j & \frac{\partial f_n}{\partial x_2}|_j & \frac{\partial f_n}{\partial x_3}|_j & \cdots & \frac{\partial f_n}{\partial x_n}|_j \end{bmatrix} \quad \text{where} \quad j = 1, ..., s \tag{19}$$

where j denotes the j^{th} state-space point.

The stiffness of the nonlinear model is often evaluated from its Jacobian using a measure such as the maximum singular value, maximum eigenvalue, condition number, or ratio of the absolute value of the eigenvalue with the greatest magnitude to the eigenvalue with the smallest magnitude (stiffness ratio) of the Jacobian. Therefore, the system identification problem can be improved to account for numerical stability of the model by adding constraints on the Jacobian of $f(x)$ in Eq. 3 evaluated at several points in the region of operation. As an example, for a system of n states, a constraint can be added on the maximum value of the stiffness ratio of the Jacobian of $f(x)$ evaluated at s points of interest in the region of operation, where the stiffness ratios are denoted as:

$$S_j = \frac{\lambda_{\max_j}}{\lambda_{\min_j}}, \quad j = 1, ..., s \tag{20}$$

with

$$\lambda_{\max_j} = \max\{|\lambda_{1j}|, |\lambda_{2j}|, ..., |\lambda_{nj}|\}, \quad j = 1, ..., s \tag{21a}$$

$$\lambda_{\min_j} = \min\{|\lambda_{1j}|, |\lambda_{2j}|, ..., |\lambda_{nj}|\}, \quad j = 1, ..., s \tag{21b}$$

where the notation λ_{ij} signifies the i^{th} ($i = 1, ..., n$) eigenvalue of the Jacobian matrix J_j, and $\lambda_{\max_j}$ and $\lambda_{\min_j}$ signify the maximum and minimum values of the magnitudes of the eigenvalues of J_j.

The numerical stability constraint to be incorporated in the PNLSS optimization problem of Eq. 18 is a bound on the maximum value of the stiffness ratio at all s points at which the Jacobian is evaluated, written as

$$R(\eta) = \max\{S_1, S_2, ..., S_s\} \le \hat{M} \tag{22}$$

where $\hat{M}$ is a number chosen to constrain the solutions to Eq. 18 to be models that are well-conditioned with respect to forward numerical integration in the region of interest.

The eigenvalues of the Jacobian matrices have to be evaluated numerically for an $n \times n$ Jacobian. To illustrate this point, we consider a two-input/two-output system with full state feedback. We define $J_1, J_2, ..., J_s$ as the Jacobians of the identified polynomial nonlinear model, evaluated at several points $j = 1, ..., s$ in the state-space region of interest. J_1 is the Jacobian evaluated at the steady-state and J_j is the Jacobian evaluated at the state-space point j where

$$J_j = \begin{bmatrix} a_j & b_j \\ c_j & d_j \end{bmatrix} \tag{23}$$

Thus, for a system with two inputs and two states, we can incorporate numerical stability constraints in the PNLSS optimization problem as follows

$$\min_{\eta\in C} \quad |x_m-x_p|_2 \tag{24a}$$

$$\text{s.t.} \quad \dot{x} = Ax+P_z(x)+Bu \tag{24b}$$

$$\frac{\lambda_{\max_j}}{\lambda_{\min_j}} \le \hat{M}, \quad j = 1, ..., s \tag{24c}$$

$$\lambda_{\max_j} = \max\{|\lambda_{1j}|, |\lambda_{2j}|\}, \quad j = 1, ..., s \tag{24d}$$

$$\lambda_{\min_j} = \min\{|\lambda_{1j}|, |\lambda_{2j}|\}, \quad j = 1, ..., s \tag{24e}$$

$$\lambda_{1j} = \frac{(a_j+d_j)}{2} + \left(\frac{(a_j+d_j)^2}{4} - (a_jd_j-b_jc_j)\right)^{1/2}, \quad j = 1, ..., s \tag{24f}$$

$$\lambda_{2j} = \frac{(a_j+d_j)}{2} - \left(\frac{(a_j+d_j)^2}{4} - (a_jd_j-b_jc_j)\right)^{1/2}, \quad j = 1, ..., s \tag{24g}$$

In this optimization problem, the cost function $\Phi(x_m - x_p)$ is taken to be the Euclidean norm of the difference between the vectors x_m and x_p.

For a 2×2 matrix, it is easy to obtain an explicit expression for the eigenvalues (e.g., Eqs. 24f and 24g). However, for an $n \times n$ matrix, the calculation of eigenvalues is not as straightforward. The characteristic polynomial could be used as an equality constraint and solved by adding additional constraints that find the roots of the characteristic polynomial numerically through a method such as Newton's Method. For certain special classes of matrices, formulas are available that allow for the explicit solution of the eigenvalues, and these could be added as constraints if the Jacobians at the evaluated points have these special forms. For example, the eigenvalues of a 3×3 matrix or of a triangular matrix of any dimension can be written explicitly. For the general case when explicit expressions for the eigenvalues may not be available, the PNLSS optimization problem for a system with n states becomes

$$\min_{\eta \in C} \quad |x_m - x_p|_2 \tag{25a}$$

$$\text{s.t.} \quad \dot{x} = Ax + P_z(x) + Bu \tag{25b}$$

$$\frac{\lambda_{\max_j}}{\lambda_{\min_j}} \leq \hat{M}, \quad j = 1, ..., s \tag{25c}$$

$$F(\eta) = 0 \tag{25d}$$

$$R(\eta) \leq 0 \tag{25e}$$

where $F(\eta)$ and $R(\eta)$ represent all constraints necessary to obtain the eigenvalues of the Jacobians J_j, $j = 1, ..., s$, and to assure numerical stability if additional constraints are desired beyond those of Eq. 25c.

Remark 3. *Several comments should be made regarding the numerical stability of a model resulting from the use of the PNLSS system identification procedure incorporating numerical stability constraints. First, the integration step size required to accurately integrate the empirical model, if it is identified using the PNLSS optimization problem with numerical stability constraints, scales with the constant $\hat{M}$ that is chosen to constrain the ratio of the maximum to minimum magnitudes of the eigenvalues; however, simulations are required to determine the integration step size needed for a given value of $\hat{M}$ so that $\hat{M}$ can then be appropriately scaled (there is no direct correlation between $\hat{M}$ and the integration step size that is known a priori or that holds for all empirical models). In addition, it may not be possible to identify a model for a given system that uses a step size as large as one would desire if the physical system for which the identification is performed behaves like a stiff system. Feasibility of the optimization problem of* Eq. 25 *is thus not ensured for all formulations of the numerical stability constraints or for all values of $\hat{M}$. Finally, though it is guaranteed that any empirical model developed using the PNLSS optimization procedure incorporating numerical stability constraints will be numerically stable to the degree specified by the numerical stability constraints, there is no guarantee that the model will accurately represent the original process. Thus, even with the proposed PNLSS optimization approach, model validation is still required, and potentially alternative stability constraints may need to be used. Regardless of the stability constraints used, however, the addition of the constraints to the PNLSS optimization problem does not substitute for model validation.*

Remark 4. *An important motivation for considering the use of numerical stability constraints is that industrial data is often noisy, which can lead to ill-conditioning of the data to be used in the minimization problem, which in turn may lead to a stiff identified model, even if the actual process dynamics are not stiff. The use of numerical stability constraints aids in identifying a non-stiff model from data that would, in the unconstrained case, be more likely to be identified to a stiff model due to measurement noise and process disturbances.*

Application of proposed method to the chemical process example

We now revisit the CSTR example described by Eq. 10 and apply the PNLSS model identification procedure once more, this time using the PNLSS approach accounting for numerical stability (Eq. 24). The previously identified ill-conditioned model of Eq. 15 is used as an initial guess for the following nonlinear optimization problem

$$\min_{\eta \in C} \quad |x_m - x_p|_2 \tag{26a}$$

$$\text{s.t.} \quad \dot{x} = Ax + P_z(x) + Bu \tag{26b}$$

$$\frac{\lambda_{\max_j}}{\lambda_{\min_j}} \leq 1000 \quad j = 1, ..., s \tag{26c}$$

$$\lambda_{\max_j} = \max\{|\lambda_{1j}|, |\lambda_{2j}|\}, \quad j = 1, ..., s \tag{26d}$$

$$\lambda_{\min_j} = \min\{|\lambda_{1j}|, |\lambda_{2j}|\}, \quad j = 1, ..., s \tag{26e}$$

$$\lambda_{1j} = \frac{(a_j + d_j)}{2} + \left(\frac{(a_j + d_j)^2}{4} - (a_j d_j - b_j c_j) \right)^{1/2} \quad j = 1, ..., s \tag{26f}$$

$$\lambda_{2j} = \frac{(a_j + d_j)}{2} - \left(\frac{(a_j + d_j)^2}{4} - (a_j d_j - b_j c_j) \right)^{1/2} \quad j = 1, ..., s \tag{26g}$$

where the modeled states in the vector x_p were determined by numerically integrating the model of Eq. 26b using Explicit Euler with a time step of $h_c = 10^{-4}$ h. For this example, the ratios of the absolute value of the eigenvalue with the greatest magnitude to the eigenvalue with the smallest magnitude of the Jacobian were evaluated at ten different points (i.e., $s = 10$) in the region of interest and were constrained to be less than 1000 to obtain a well-conditioned model with respect to the integration step of $h_c = 10^{-4}$ h. The nonlinear model of the CSTR (in continuous-time) that is identified by the optimization problem of Eq. 26 is:

$$\frac{dx_1}{dt} = -34.00x_1 - 0.495x_2 - 5.22x_1^2 - 0.902x_1x_2 - 0.0078x_2^2 - 4.6u_1 - 0.000008u_2 \tag{27a}$$

$$\frac{dx_2}{dt} = 1436x_1 + 18x_2 + 432x_1^2 + 43.6x_1x_2 + 0.376x_2^2 - 11u_1 + 0.00567u_2 \tag{27b}$$

We now compare the numerical stability of the model of Eq. 27 with that of the model of Eq. 15. We recall the results of Figures 1 and 2, which showed that a step size of 10^{-4} h was inadequate for sufficient model accuracy so that decreasing the step size was necessary to obtain a more accurate integration. For the model of Eq. 27, however, a step size of 10^{-4} h is

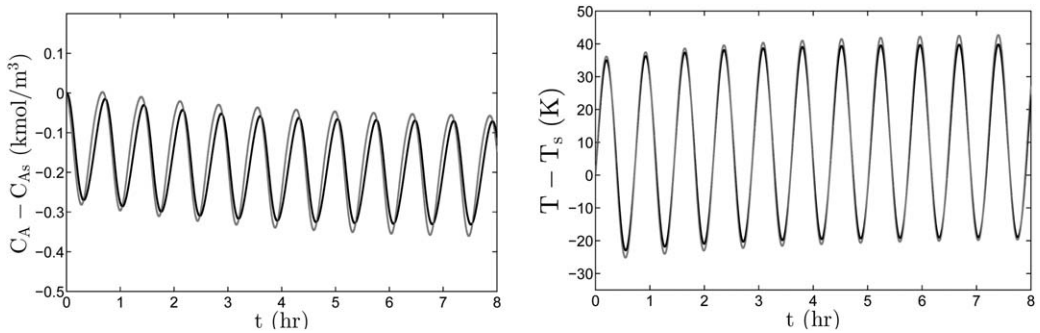

Figure 3. State trajectories of the first-principles CSTR model of Eq. 10 (black trajectory) and the identified PNLSS model of Eq. 27, $h_c = 10^{-4}$ h (gray trajectory) when the heat rate and concentration inputs are varied sinusoidally with amplitudes 55,000 kJ/h and 0.25 kmol/m^3, respectively, and both with frequency 8.72 rad/h.

sufficient. This is shown in Figure 3, a plot of the state trajectories when the Explicit Euler method is used to numerically integrate the model of Eq. 27 with step size $h_c = 10^{-4}$ h and a sinusoidal input to the system. Figure 3 shows that the empirical model of Eq. 27 resulting from the PNLSS identification approach with numerical stability constraints is able to predict the nonlinear dynamics of the CSTR system of Eq. 10 accurately with a larger step size than was needed when using the model of Eq. 15. Examining the error in concentration and temperature defined according to Eqs. 16 and 17 for the model of Eq. 27 further illustrates this point. The average error in concentration for the model of Eq. 27 over eight hours of operation with an integration step size of 10^{-4} h is 2.0276×10^{-4}, and the average error in the temperature is 0.2342. The concentration error with this larger step size for Eq. 27 is on the same order of magnitude as the concentration error using Eq. 15 with a step size of 10^{-6} h, and the temperature error is almost an order of magnitude smaller.

The average computation time for each hour of simulation of the model of Eq. 27 with the 10^{-4} h integration step is 0.986 CPU seconds which is more than 21 times faster than using Eq. 15 with the step size of $h_c = 10^{-6}$ h for which each hour of simulation required 21.58 CPU seconds. This shows that with a much larger integration time step, the model of Eq. 27 was able to accurately predict the nonlinear CSTR behavior.

A step input and impulse input were used to further validate the model of Eq. 27. The responses for the polynomial model of Eq. 27 and the first-principles model of Eq. 10 to a step change in u_2 and an impulse input of u_1 are very close, as is shown in Figures 4 and 5.

EMPC Using Well-Conditioned Nonlinear Models

The formulation of LEMPC incorporating the PNLSS model and the stability of a nonlinear process in closed-loop with this LEMPC will now be developed in steps through a series of propositions and a theorem. The first step will be to develop the stability of the nonlinear process of Eq. 1 when a Lyapunov-based controller derived from the empirical PNLSS model of Eq. 3 is applied to it, which is now addressed.

Lyapunov-based control using empirical models

The empirical nonlinear model of Eq. 3 is assumed to be stabilizable such that a state feedback controller $h_{NL}(x)$ exists that can make the origin of the empirical nonlinear system of Eq. 3 under $h_{NL}(x)$ locally exponentially stable. We will further assume that h_{NL} is locally Lipschitz on R^n such that one can find a constant $K > 0$ to bound the value of h_{NL} ($|h_{NL}(x)| < K|x|$ for all $x \in R^n$). When the input for the system of Eq. 1 under nominal operation is the controller $h_{NL}(x)$ that is designed based on the empirical model of Eq. 3, closed-loop stability depends on whether the z^{th} order Taylor series expansion of the nominal model is sufficiently close to the polynomial empirical model expanded to the same order z. It also depends on the effect of the higher order terms (nonlinear terms of order $z+1$ and higher) on the trajectories of the system of Eq. 1. In the following, we introduce the Taylor series of the right-hand side of Eq. 1 in a compact form. To simplify the notation throughout this section, the right-hand side of Eq. 1 is denoted as follows

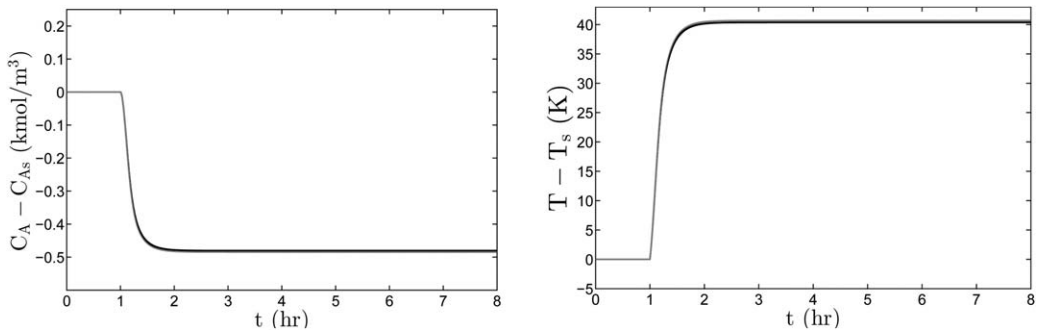

Figure 4. Step responses of the first-principles CSTR model of Eq. 10 (black trajectory) and of the identified PNLSS model of Eq. 27 (gray trajectory) when, after 1 h of operation at the process steady-state, the heat rate (u_2) is suddenly increased by 20,000 kJ/h.

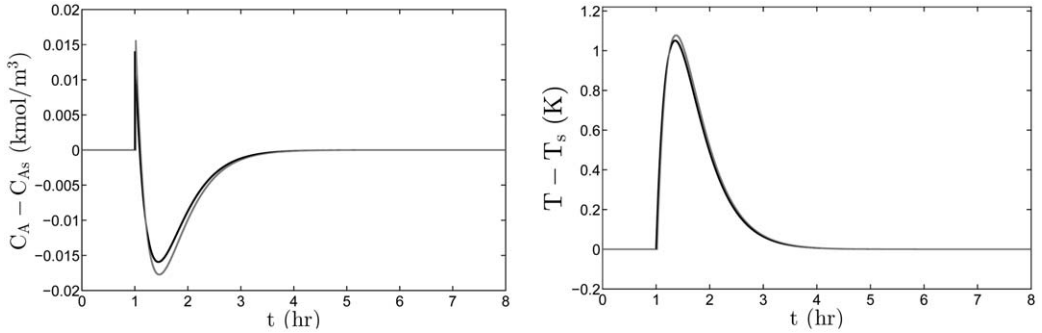

Figure 5. Impulse responses of the first-principles CSTR model of Eq. 10 (black trajectory) and of the identified PNLSS model of Eq. 27 (gray trajectory). The impulse was applied to the systems after 1 h of operation at the process steady-state, and the impulse was numerically simulated as a rectangular pulse input in u_1 of magnitude 1 kmol/m^3 that was applied for 72 s.

$$\tilde{f}(x(t),w(t),u(t)) := f_p(x(t),w(t)) + \tilde{G}(x(t),w(t))u(t) \quad (28)$$

To obtain the Taylor series of the entire vector function $\tilde{f} : R^n \times R^l \times R^m \to R^n$, the Taylor series expansion of each function $\tilde{f}_i, i = 1, ..., n$ is taken individually. The Taylor series expansion of the function $\tilde{f}_i$ of the nominal model ($w(t) = 0$) of Eq. 28 around an equilibrium point $x = 0$ with $u = 0$ is

$$\tilde{f}_i(x,0,u) = \bar{a}_i x + \frac{1}{2!}\sum_{i=1}^{n}\sum_{q=1}^{n}\frac{\partial^2 \tilde{f}_i}{\partial x_i \partial x_q}(0,0,0)x_i x_q + ... + \bar{b}_i u + \frac{1}{2!}\sum_{\Gamma=1}^{m}\sum_{v=1}^{m}\frac{\partial^2 \tilde{f}_i}{\partial u_\Gamma \partial u_v}(0,0,0)u_\Gamma u_v + ... \quad (29)$$

where

$$\bar{a}_i = \left[\frac{\partial \tilde{f}_i}{\partial x_1}(0,0,0) \quad \frac{\partial \tilde{f}_i}{\partial x_2}(0,0,0) \quad \frac{\partial \tilde{f}_i}{\partial x_3}(0,0,0) \ ... \ \frac{\partial \tilde{f}_i}{\partial x_n}(0,0,0)\right] \quad (30)$$

$$\bar{b}_i = \left[\frac{\partial \tilde{f}_i}{\partial u_1}(0,0,0) \quad \frac{\partial \tilde{f}_i}{\partial u_2}(0,0,0) \quad \frac{\partial \tilde{f}_i}{\partial u_3}(0,0,0) \ ... \ \frac{\partial \tilde{f}_i}{\partial u_m}(0,0,0)\right] \quad (31)$$

Now, all terms in the Taylor series polynomial containing derivatives of $\tilde{f}_i$ of order $z + 1$ and higher with respect to x are disregarded and only the linear terms with respect to the input u are kept because the model of Eq. 28 is affine in u. To simplify the notation of the remaining polynomial terms, we define $\tilde{g}_i(x)$ as

$$\tilde{g}_i(x) = \hat{g}_i \Lambda(x) \quad (32a)$$

$$\Lambda(x) = [x_1^2 \quad x_1 x_2 \ ... \ x_n^z]^T \quad (32b)$$

where the vector $\Lambda(x)$ contains nonlinear monomials in x of order two and higher up to a chosen order z. The coefficients of these nonlinear terms in x are placed in the vector $\hat{g}_i$. As an example, when $n = 2$ and $z = 3$, $\Lambda(x)$ and $\hat{g}_1$ have the following form

$$\hat{g}_1 = \left[\frac{1}{2}\frac{\partial^2 \tilde{f}_1}{\partial x_1^2} \quad \frac{\partial^2 \tilde{f}_1}{\partial x_1 \partial x_2} \quad \frac{1}{2}\frac{\partial^2 \tilde{f}_1}{\partial x_2^2} \quad \frac{1}{6}\frac{\partial^3 \tilde{f}_1}{\partial x_1^3} \quad \frac{1}{2}\frac{\partial^3 \tilde{f}_1}{\partial x_1^2 \partial x_2} \quad \frac{1}{2}\frac{\partial^3 \tilde{f}_1}{\partial x_1 \partial x_2^2} \quad \frac{1}{6}\frac{\partial^3 \tilde{f}_1}{\partial x_1^3}\right]_{(0,0,0)} \quad (33)$$

$$\Lambda(x) = [x_1^2 \quad x_1 x_2 \quad x_2^2 \quad x_1^3 \quad x_1^2 x_2 \quad x_1 x_2^2 \quad x_2^3]^T \quad (34)$$

Repeating the same procedure to calculate the Taylor series for all $\tilde{f}_i$, $i = 1, ..., n$ functions, and defining the matrices $\bar{A}$ and $\bar{B}$ and the vector $\bar{G}_z(x)$ to have row vectors $\bar{a}_i$, $\tilde{g}_i(x)$, and $\bar{b}_i$, $i = 1, ..., n$, respectively, the Taylor series approximation of the vector function $\tilde{f}$ can be represented in the following compact notation

$$\tilde{f}(x,0,u) \approx \bar{A}x + \bar{G}_z(x) + \bar{B}u \quad (35)$$

where $\bar{A}$ and $\bar{B}$ represent the coefficients of the linear terms in x and u respectively and $\bar{G}_z(x)$ is a nonlinear vector function that includes terms of order two and higher. The subscript z is used to indicate that $\bar{G}_z(x)$ is a z^{th} order polynomial vector function. We will now develop a proposition that shows that the state feedback controller $h_{NL}(x)$ is locally robust to the plant-model mismatch and the effect of nonlinearities (of order $z + 1$ and higher) when the process model is close to the Taylor series expansion of the actual nonlinear model. To facilitate this development, we define the matrix of coefficients of the nonlinear terms in $\bar{G}_z(x)$ as $\hat{G}_z$ (the row vectors of $\hat{G}_z$ are $\hat{g}_i$, $i = 1, ..., n$). The following proposition provides conditions for exponential stability of the actual nonlinear system under a controller h_{NL} designed based on a polynomial approximation of the actual process model.

Proposition 1. *Under the assumption that the origin of the closed-loop system of* Eq. 3 *under the controller $h_{NL}(x)$ is locally exponentially stable and there exist $W > 0$ and $\delta > 0$ such that*

$$||(\bar{A} - A) + (\hat{G}_z - E)||W + ||\bar{B} - B||K \le \delta \quad (36)$$

then there exists $\hat{\rho} > 0$ such that the origin of the nominal closed-loop system of Eq. 1 *under $h_{NL}(x)$ is exponentially stable for all $x \in \Omega_{\hat{\rho}}$.*

Proof. To prove exponential stability of the origin of Eq. 1 for sufficiently small $\hat{\rho}$ and δ, it is sufficient to show that a Lyapunov function exists for that system in closed-loop with the controller $h_{NL}(x)$. To prove the existence of such a function, we first note that the exponential stability of the origin of Eq. 3 under the controller $h_{NL}(x)$ guarantees that there is a continuously differentiable Lyapunov function $\hat{V} : R^n \to R_+$ that satisfies the following inequalities[49]

$$c_1|x|^2 \le \hat{V}(x) \le c_2|x|^2 \quad (37a)$$

$$\frac{\partial \hat{V}(x)}{\partial x}(Ax+P_z(x)+Bh_{NL}(x)) \leq -c_3|x|^2 \tag{37b}$$

$$\left|\frac{\partial \hat{V}(x)}{\partial x}\right| \leq c_4|x| \tag{37c}$$

for all $x \in D_{NL}$ where c_1, c_2, c_3, and c_4 are positive constants. These are not necessarily the same positive constants as in Eq. 2, but the same constants have been used here to simplify the subsequent notation.
We next define

$$q(x) := \tilde{f}(x, h_{NL}(x), 0) - \bar{A}x - \bar{G}_z(x) - \bar{B}h_{NL}(x) \tag{38}$$

and consider

$$\dot{x} = Ax+P_z(x)+Bh_{NL}(x)+\tilde{f}(x, h_{NL}(x), 0)-Ax-P_z(x)-Bh_{NL}(x) \tag{39}$$

Using Eqs. 37b and 37c, the time-derivative of $\hat{V}$ along the state of the system of Eq. 39 is bounded by

$$\begin{aligned}\dot{\hat{V}} \leq -c_3|x|^2+c_4|x|(|(\bar{A}-A)x+(\bar{G}_z(x)-P_z(x)) \\ +(\bar{B}-B)h_{NL}(x)|+|q(x)|)\end{aligned} \tag{40}$$

for all $x \in D_{NL}$. Using boundedness of vector fields and the fact that the $h_{NL}(x)$ controller is locally Lipschitz, there exist constants $W > 0$ and $K > 0$ such that

$$\begin{aligned}\dot{\hat{V}} \leq -c_3|x|^2+c_4|x|(((|(\bar{A}-A) \\ +(\hat{G}_z-E)||W+||\bar{B}-B||K)|x|+|q(x)|)\end{aligned} \tag{41}$$

for all $x \in B_{r\prime} = \{x \in R^n : |x| \leq r\prime\}$ where $r\prime$ is any $r\prime > 0$ such that $B_{r\prime} \subset D_{NL}$. If the condition of Eq. 36 is satisfied, there exits a $\delta > 0$ such that

$$\dot{\hat{V}} \leq -c_3|x|^2+c_4\delta|x|^2+c_4|x||q(x)| \tag{42}$$

for all $x \in B_{r\prime}$, and since $q(x)$ vanishes near the origin and contains terms of order $z+1$ and higher in x, there exists a $\gamma > 0$ such that

$$|q(x)| < \gamma|x|^{z+1} \tag{43}$$

for all $x \in B_{r\prime}$. Thus

$$\dot{\hat{V}} \leq -c_3|x|^2+c_4\delta|x|^2+c_4\gamma|x|^{z+2} \tag{44}$$

for all $x \in B_{r\prime}$. For any $B_r \subset B_{r\prime}$, the time-derivative of $\hat{V}$ can be bounded by

$$\dot{\hat{V}} \leq -c_3|x|^2+c_4(\delta+\gamma r^z)|x|^2 \tag{45}$$

for all $x \in B_r$ where $r < r\prime$. If $\delta > 0$ and $r > 0$ are chosen to satisfy $c_3/c_4 > (\delta+\gamma r^z)$, then there exists a $\hat{c}_3 > 0$ such that

$$\dot{\hat{V}} = \frac{\partial \hat{V}(x)}{\partial x}\left(\tilde{f}(x, h_{NL}(x), 0)\right) \leq -\hat{c}_3|x|^2 \tag{46}$$

for all $|x| \leq r$. Let $\Omega_{\hat{\rho}}$ with $\hat{\rho} > 0$ be the forward invariant set such that $\hat{\rho} \leq \min\{\hat{V}(x) : |x| = r\}$ and this ends the proof. ■

Remark 5. *Even though this conservative result holds locally, when higher order terms are used to better capture the nonlinear behavior in a practical setting, the region $\Omega_{\hat{\rho}}$ could be expanded as will be demonstrated in the example.*

Lyapunov-based EMPC formulation with well-conditioned empirical models

The formulation of EMPC to be used in this work is LEMPC,[2,55] a receding horizon EMPC strategy that incorporates stability constraints based on an explicit stabilizing controller for a model of the nominal process. LEMPC uses a model of the process dynamics to predict the evolution of the process states with time. The LEMPC developed here will be implemented with sampling period Δ and prediction horizon N, and the stability constraints will be based on the stability region and Lyapunov function $\hat{V}(x)$ for the system of Eq. 3 under the stabilizing controller $h_{NL}(x)$. In addition, the process model to be incorporated in LEMPC will be the nonlinear PNLSS empirical model. The LEMPC formulation is similar to that derived in Ref. 55 using an empirical model. The LEMPC optimization problem incorporating the PNLSS empirical model is

$$\min_{u \in S(\Delta)} \quad \int_{t_k}^{t_{k+N}} L_e(\tilde{x}(\tau), u(\tau))\, d\tau \tag{47a}$$

$$\text{s.t.} \quad \dot{\tilde{x}}(t) = A\tilde{x}+P_z(\tilde{x})+Bu \tag{47b}$$

$$\tilde{x}(t_k) = x(t_k) \tag{47c}$$

$$u(t) \in U, \ \forall \ t \in [t_k, t_{k+N}) \tag{47d}$$

$$\hat{V}(\tilde{x}(t)) \leq \hat{\rho}_e, \ \forall \ t \in [t_k, t_{k+N}), \quad \text{if} \ \ x(t_k) \in \Omega_{\hat{\rho}_e} \tag{47e}$$

$$\begin{aligned}&\frac{\partial \hat{V}(x(t_k))}{\partial x}(Ax(t_k)+P_z(x(t_k))+Bu(t_k)) \\ &\leq \frac{\partial \hat{V}(x(t_k))}{\partial x}(Ax(t_k)+P_z(x(t_k))+Bh_{NL}(x(t_k))), \\ &\text{if} \ \ x(t_k) \notin \Omega_{\hat{\rho}_e}\end{aligned} \tag{47f}$$

where the optimization variable is the process input vector u for every sampling period of length Δ in the prediction horizon (denoted by $u \in S(\Delta)$ where $S(\Delta)$ represents the family of piecewise constant functions with period Δ). To solve for this optimization variable, the LEMPC minimizes a cost function representing the process economics (Eq. 47a, where $L_e(x, u)$ is the stage cost) and ensures that the calculated values of u are maintained within the specified limits on the available control action (Eq. 47d). The LEMPC receives a measurement of the process states at time t_k (the time at the beginning of a sampling period) and incorporates this through Eq. 47c as the initial condition in the PNLSS process model of Eq. 47b. The prediction of the process state from Eq. 47b is denoted as $\tilde{x}$. The PNLSS process model is used to predict future states of the process system to ensure that they are constrained by the mode 1 and mode 2 Lyapunov-based constraints of Eqs. 47e and 47f, respectively.

The mode 1 constraint is used to promote dynamic off-steady-state operation of the process to achieve the greatest profit possible, and is active when the states are maintained within a subset of the stability region $\Omega_{\hat{\rho}}$ that is referred to as $\Omega_{\hat{\rho}_e}$ for which states starting within this subset are guaranteed to be maintained in the stability region $\Omega_{\hat{\rho}}$ for all time. Process disturbances or plant-model mismatch may cause the actual process trajectories to enter the region $\Omega_{\hat{\rho}} \setminus \Omega_{\hat{\rho}_e}$, in which case the mode 2 LEMPC constraint becomes active to drive the process states back into $\Omega_{\hat{\rho}_e}$ within a finite number of sampling periods.

Stability analysis

In this section, we examine stability of the closed-loop process of Eq. 1 under LEMPC incorporating the empirical model

derived from PNLSS with numerical stability constraints. We begin by noting several bounds on the process models of Eqs. 1 and 3 and of the derivatives of Lyapunov functions along the closed-loop trajectories of these systems. Because it is assumed that $\tilde{f}(\cdot,\cdot,\cdot)$ in Eq. 1 is locally Lipschitz and that the Lyapunov function $\hat{V}$ is continuously differentiable, the following inequalities hold for all $x_1,\ x_2 \in \Omega_{\hat{\rho}}$, $u \in U$ and $|w| \leq \theta$

$$|\tilde{f}(x_1,u,w)-\tilde{f}(x_2,u,0)| \leq L_x|x_1-x_2|+L_w|w| \tag{48}$$

$$\left|\frac{\partial \hat{V}(x_1)}{\partial x}\tilde{f}(x_1,u,w)-\frac{\partial \hat{V}(x_2)}{\partial x}\tilde{f}(x_2,u,0)\right| \leq L'_x|x_1-x_2|+L'_w|w| \tag{49}$$

where L_x, L_w, L'_x, and L'_w are positive constants. The Lipschitz property of $\tilde{f}$, combined with the bounds on u and w, establishes the existence of a constant $M>0$ such that

$$|\tilde{f}(x,u,w)| \leq M \tag{50}$$

for all $x \in \Omega_{\hat{\rho}}$, $u \in U$ and $|w| \leq \theta$ since $\Omega_{\hat{\rho}}$ and U are compact sets.

The polynomial model of Eq. 3 and the time-derivative of the Lyapunov function along its state are similarly bounded by $M_{NL}>0$ and $L_{NL}>0$

$$|Ax_1+P_z(x_1)+Bu| \leq M_{NL} \tag{51}$$

$$\left|\frac{\partial \hat{V}(x_1)}{\partial x}(Ax_1+P_z(x_1)+Bu)-\frac{\partial \hat{V}(x_2)}{\partial x}(Ax_2+P_z(x_2)+Bu)\right| \leq L_{NL}|x_1-x_2| \tag{52}$$

for all $x_1, x_2 \in \Omega_{\hat{\rho}}$ and $u \in U$.

This next proposition defines a bound on the difference between the state of the actual process of Eq. 1 in the presence of disturbances $w(t)$ and the state predicted from the empirically derived PNLSS model of Eq. 3 over a time interval of length T.

Proposition 2. *The solutions of the following dynamic equations are denoted as x(t) and* $\hat{x}(t)$

$$\dot{x}(t) = \tilde{f}(x(t),u(t),w(t)), \quad x(0)=x_0 \tag{53}$$

$$\dot{\hat{x}}(t) = A\hat{x}(t)+P_z(\hat{x}(t))+Bu(t), \quad \hat{x}(0)=x_0 \tag{54}$$

where $u(t) \in U$ *and* $|w(t)| \leq \theta$ *for all* $t \in [0,T]$ *with initial condition* $x(0)=\hat{x}(0)=x_0 \in \Omega_{\hat{\rho}}$. *If* $x(t),\ \hat{x}(t) \in \Omega_{\hat{\rho}}$ *for all* $t \in [0,T]$, *then the difference between x(T) and* $\hat{x}(T)$ *is bounded by the function* $f_w(\cdot)$

$$|x(T)-\hat{x}(T)| \leq f_w(T) := \frac{L_w\theta+M_{\text{err}}}{L_x}\left(e^{L_xT}-1\right) \tag{55}$$

where M_{err} *bounds the difference between right-hand sides of* Eq. 53 *with* $w(t)\equiv 0$ *and* Eq. 54

$$|\tilde{f}(\hat{x},u,0)-(A\hat{x}+P_z(\hat{x})+Bu)| \leq M_{\text{err}} \tag{56}$$

for all $\hat{x} \in \Omega_{\hat{\rho}}$ *and* $u \in U$.

Proof. We will first define $e(t)$ to be the difference $x(t)-\hat{x}(t)$, such that its time-derivative is $\dot{e}(t)=\dot{x}(t)-\dot{\hat{x}}(t)$. Per Eqs. 53 and 54, the initial condition for this differential equation is $e(0)=0$. Substituting the definitions of $\dot{x}(t)$ and $\dot{\hat{x}}(t)$ from Eqs. 53 and 54 in the definition of $\dot{e}(t)$ produces the following inequality

$$\begin{aligned}|\dot{e}(t)| &= |\tilde{f}(x(t),u(t),w(t))-(A\hat{x}(t)+P_z(\hat{x}(t))+Bu(t))| \\ &\leq |\tilde{f}(x(t),u(t),w(t))-\tilde{f}(\hat{x}(t),u(t),0)| \\ &\quad +|\tilde{f}(\hat{x}(t),u(t),0)-(A\hat{x}(t)+P_z(\hat{x}(t))+Bu(t))|\end{aligned} \tag{57}$$

for all $x,\ \hat{x}$ contained in $\Omega_{\hat{\rho}}$. From the bounds in Eqs. 50 and 51 above and the fact that x and u are in compact sets, a constant $M_{\text{err}}>0$ exists such that

$$|\tilde{f}(\hat{x},u,0)-(A\hat{x}+P_z(\hat{x})+Bu)| \leq M_{\text{err}} \tag{58}$$

for all $\hat{x} \in \Omega_{\hat{\rho}}$ and all $u \in U$. Using this bound in Eq. 57 along with the bound from Eq. 48 and $|w(t)| \leq \theta$, the following is derived for all $t \in [0,T]$

$$\begin{aligned}|\dot{e}(t)| &\leq L_x|x(t)-\hat{x}(t)|+L_w|w(t)|+M_{\text{err}} \\ &\leq L_x|e(t)|+L_w\theta+M_{\text{err}}\end{aligned} \tag{59}$$

Integration is then performed on the differential equation in Eq. 59 between $t=0$ and $t=T$

$$\int_0^T \frac{|\dot{e}(t)|}{L_x|e(t)|+L_w\theta+M_{\text{err}}}\,dt \leq T \tag{60}$$

which gives the following equation for $|e(T)|$, with $x(T)$, $\hat{x}(T) \in \Omega_{\hat{\rho}}$

$$|e(T)| = |x(T)-\hat{x}(T)| \leq \frac{L_w\theta+M_{\text{err}}}{L_x}\left(e^{L_xT}-1\right) \tag{61}$$

This completes the proof of Proposition 2.

The following proposition is proved in Ref. 56 and states that the difference between the values of a Lyapunov function evaluated at any two different points in $\Omega_{\hat{\rho}}$ is bounded. ■

Proposition 3. (c.f. Ref. 56) *Consider the continuously differentiable Lyapunov function* $\hat{V}(x)$ *that satisfies the inequalities of* Eq. 37. *There exists a quadratic function* $f_V(\cdot)$ *such that*

$$\hat{V}(x_1) \leq \hat{V}(x_2)+f_V(|x_1-x_2|) \tag{62}$$

for all $x_1,\ x_2 \in \Omega_{\hat{\rho}}$ where

$$f_V(s) := \frac{c_4\sqrt{\hat{\rho}}}{\sqrt{c_1}}s+\beta s^2 \tag{63}$$

and β *is a positive constant.*

The above propositions will now be used to show that firstly, there exists a feedback control law h_{NL} that meets the requirements of Eq. 37 that can stabilize the closed-loop system of Eq. 1, and secondly, that this has implications for the stability properties of an LEMPC based on the stability region derived from the use of this feedback control law. To develop the type of stability that the feedback control law can provide, we first note that when h_{NL} meeting Eq. 37 is applied continuously to the system of Eq. 3, it exponentially stabilizes the origin of the closed-loop system. However, for the LEMPC control problem at hand, the control laws will be implemented in sample-and-hold, using synchronous sampling at times $t_k = k\Delta$, $k=0,1,\ldots$. When using a sufficiently small sampling period $\Delta>0$, the control law h_{NL} implemented in sample-and-hold can practically stabilize the origin of Eq. 3, meaning that it can drive the state trajectories to a small neighborhood of the origin $\Omega_{\hat{\rho}_{\min}}$ and maintain them there.[56] It has previously been stated that the Lyapunov-based constraints in LEMPC are able to ensure

that the closed-loop state trajectories using mode 1 operation are maintained in the stability region $\Omega_{\hat{\rho}}$ and that the origin is practically stable in mode 2; this, however, implies that feasible solutions to the LEMPC exist, which is only the case for mode 1 operation when $\hat{\rho}_e \geq \hat{\rho}_{\min}$. The following proposition states that when $\hat{\rho}_e$ is restricted in this manner, the state trajectories $\hat{x}(t)$ for the closed-loop system of Eq. 54 under the control law h_{NL} in sample-and-hold are always bounded in $\Omega_{\hat{\rho}_e}$, which is necessary for feasibility of mode 1 operation of LEMPC, and are ultimately bounded in $\Omega_{\hat{\rho}_{\min}}$.

Proposition 4. *Consider the sampled-data system resulting from the system of* Eq. 54 *under the controller* $h_{NL}(\hat{x})$ *that satisfies the inequalities of* Eq. 37 *implemented in a sample-and-hold fashion. Let* $\Delta > 0$, $\hat{\epsilon}_s > 0$, *and* $\hat{\rho}_e \geq \hat{\rho}_{\min} \geq \hat{\rho}_s > 0$ *satisfy*

$$-\frac{c_3}{c_2}\hat{\rho}_s + L_{NL}M_{NL}\Delta \leq -\hat{\epsilon}_s/\Delta \tag{64}$$

and

$$\hat{\rho}_{\min} := \max\{\hat{V}(\hat{x}(t+\Delta)) \ : \ \hat{V}(\hat{x}(t)) \leq \hat{\rho}_s\} \tag{65}$$

If $\hat{x}(0) \in \Omega_{\hat{\rho}_e}$, then $\hat{x}(t) \in \Omega_{\hat{\rho}_e}$ for all $t \geq 0$ and

$$\hat{V}(\hat{x}(t_{k+1})) - \hat{V}(\hat{x}(t_k)) \leq -\hat{\epsilon}_s \tag{66}$$

for $\hat{x}(t_k) \in \Omega_{\hat{\rho}_e} \setminus \Omega_{\hat{\rho}_s}$ *and* $\hat{x}(t)$ *is ultimately bounded in* $\Omega_{\hat{\rho}_{\min}}$.

Proof. The proposition considers the state trajectories of the system of Eq. 54, starting from $\hat{x}(0) \in \Omega_{\hat{\rho}_e}$, when the control law $h_{NL}(\hat{x})$ is implemented in sample-and-hold. This sample-and-hold implementation will be denoted as $h_{NL}(\hat{x}(t_k))$, with $t \in [t_k, t_{k+1})$, $k = 0, 1, \ldots$ with $t_0 = 0$, to represent the value of h_{NL} held for a time period of length Δ based on a measurement of the state $\hat{x}$ at time t_k. Using this notation and the inequality of Eq. 37b that holds at each sampling time, the following holds

$$\frac{\partial \hat{V}(\hat{x}(t_k))}{\partial \hat{x}}(A\hat{x}(t_k) + P_z(\hat{x}(t_k)) + Bh_{NL}(\hat{x}(t_k))) \leq -c_3|\hat{x}(t_k)|^2 \tag{67}$$

The inequality of Eq. 67 can be used with the inequality of Eq. 52 to bound the time-derivative of the Lypaunov function for all $\tau \in [t_k, t_{k+1})$ as follows (the notation for the input is abbreviated as $\hat{u}(t_k) := h_{NL}(\hat{x}(t_k))$)

$$\begin{aligned}
&\frac{\partial \hat{V}(\hat{x}(\tau))}{\partial \hat{x}}(A\hat{x}(\tau) + P_z(\hat{x}(\tau)) + B\hat{u}(t_k)) \\
&\quad = \frac{\partial \hat{V}(\hat{x}(\tau))}{\partial \hat{x}}(A\hat{x}(\tau) + P_z(\hat{x}(\tau)) + B\hat{u}(t_k)) \\
&\quad - \frac{\partial \hat{V}(\hat{x}(t_k))}{\partial \hat{x}}(A\hat{x}(t_k) + P_z(\hat{x}(t_k)) + B\hat{u}(t_k)) \\
&\quad + \frac{\partial \hat{V}(\hat{x}(t_k))}{\partial \hat{x}}(A\hat{x}(t_k) + P_z(\hat{x}(t_k)) + B\hat{u}(t_k)) \\
&\quad \leq L_{NL}|\hat{x}(\tau) - \hat{x}(t_k)| - c_3|\hat{x}(t_k)|^2
\end{aligned} \tag{68}$$

Because the solutions of Eq. 54 are continuous in the compact set $\Omega_{\hat{\rho}_e}$, a discretization of the time-derivative of $\hat{x}$ defined according to Eq. 54 for a sufficiently small time Δ, combined with the inequality in Eq. 51, yields the following bound for $\tau \in [t_k, t_{k+1}]$

$$|\hat{x}(\tau) - \hat{x}(t_k)| \leq M_{NL}\Delta \tag{69}$$

Substituting Eq. 69 into Eq. 68 gives for $\tau \in [t_k, t_{k+1})$

$$\begin{aligned}
&\frac{\partial \hat{V}(\hat{x}(\tau))}{\partial \hat{x}}(A\hat{x}(\tau) + P_z(\hat{x}(\tau)) + B\hat{u}(t_k)) \\
&\quad \leq -c_3|\hat{x}(t_k)|^2 + L_{NL}M_{NL}\Delta
\end{aligned} \tag{70}$$

We now use these results to show that $\hat{x}(t) \in \Omega_{\hat{\rho}_e}$ for all $t \geq 0$ when $\hat{x}(0) \in \Omega_{\hat{\rho}_e}$, $\hat{\rho}_s > 0$, $\hat{\rho}_{\min} > 0$, $\hat{\epsilon}_s > 0$, and $\hat{\rho}_e \geq \hat{\rho}_{\min}$ satisfy Eqs. 64 and 65 with a sufficiently small $\Delta > 0$. We first examine the case when $\hat{x}(t_k) \in \Omega_{\hat{\rho}_e} \setminus \Omega_{\hat{\rho}_s}$ (and $\hat{x}(\tau) \in \Omega_{\hat{\rho}_e}$ for $\tau \in [t_k, t_{k+1})$). In this case, Eq. 70 and Eq. 37a are combined to give

$$\frac{\partial \hat{V}(\hat{x}(\tau))}{\partial \hat{x}}(A\hat{x}(\tau) + P_z(\hat{x}(\tau)) + B\hat{u}(t_k)) \leq -\frac{c_3}{c_2}\hat{\rho}_s + L_{NL}M_{NL}\Delta \tag{71}$$

for $\tau \in [t_k, t_{k+1})$. Since we assume that Eq. 64 is met

$$\frac{\partial \hat{V}(\hat{x}(\tau))}{\partial \hat{x}}(A\hat{x}(\tau) + P_z(\hat{x}(\tau)) + B\hat{u}(t_k)) \leq -\hat{\epsilon}_s/\Delta \tag{72}$$

for $\tau \in [t_k, t_{k+1})$. Using continuity of the solutions of Eq. 54 in a compact set and integrating Eq. 72 for $\tau \in [t_k, t_{k+1}]$ proves that the bound of Eq. 66 holds and further shows that the Lyapunov function is decreasing for $\tau \in [t_k, t_{k+1}]$, which proves that $\hat{x}(t)$ is maintained in $\Omega_{\hat{\rho}_e}$ during this time period as guaranteed by the proposition

$$\begin{aligned}
&\hat{V}(\hat{x}(t_{k+1})) \leq \hat{V}(\hat{x}(t_k)) - \hat{\epsilon}_s, \\
&\hat{V}(\hat{x}(\tau)) \leq \hat{V}(\hat{x}(t_k)), \quad \forall \ \tau \in [t_k, t_{k+1}]
\end{aligned} \tag{73}$$

We now prove ultimate boundedness of the state trajectories in $\Omega_{\hat{\rho}_{\min}}$ by considering $\hat{x}(t_k) \in \Omega_{\hat{\rho}_s}$. Because the proof for $\hat{x}(t_k) \in \Omega_{\hat{\rho}_e} \setminus \Omega_{\hat{\rho}_s}$ shows that the Lyapunov function continues to decrease with time in that set, the trajectories eventually enter $\Omega_{\hat{\rho}_s}$. From the definition of $\Omega_{\hat{\rho}_{\min}}$ in Eq. 65, once the state trajectories enter $\Omega_{\hat{\rho}_{\min}}$, they are ultimately bounded in this set. This completes the proof of Proposition 4 and shows that for appropriately chosen parameters $\hat{\rho}_s$, $\hat{\epsilon}_s$, $\hat{\rho}_e$, and Δ, an explicit stabilizing controller exists for the system of Eq. 54 that, when implemented in sample-and-hold, can render the set $\Omega_{\hat{\rho}_e}$ forward invariant for any initial state in $\Omega_{\hat{\rho}_e}$. ■

Propositions 2–4 are now combined to give a theorem that shows that the LEMPC applied to the system of Eq. 1 using the empirical PNLSS model of Eq. 3 requests control actions that maintain boundedness of the closed-loop state within $\Omega_{\hat{\rho}}$ under appropriate conditions.

Theorem 1. *Consider the closed-loop system of* Eq. 1 *under the LEMPC of* Eq. 47 *based on the controller* $h_{NL}(x)$ *that satisfies the inequalities of* Eq. 37. *Let* $\epsilon_w > 0$, $\Delta > 0$, $N \geq 1$, *and* $\hat{\rho} > \hat{\rho}_e > 0$ *satisfy*

$$-\frac{\hat{c}_3}{c_2}\hat{\rho}_e + L_x'M\Delta + L_w'\theta \leq -\epsilon_w/\Delta \tag{74}$$

$$\hat{\rho}_e \leq \hat{\rho} - f_V(f_w(\Delta)) \tag{75}$$

If $x(0) \in \Omega_{\hat{\rho}}$ *and the conditions of* Proposition 1 *and* Proposition 4 *are satisfied, then the state trajectory x(t) of the closed-loop system is always bounded in* $\Omega_{\hat{\rho}}$ *for* $t \geq 0$.

Proof. In *Part 1* of this proof, we show that the LEMPC optimization problem is recursively feasible if $x(t)$ does not leave $\Omega_{\hat{\rho}}$, and in *Part 2*, we prove boundedness of the states of the closed-loop system in $\Omega_{\hat{\rho}}$. ■

Part 1. For all $x(t_k) \in \Omega_{\hat{\rho}_e}$ when all conditions in Proposition 4 are met, the optimization problem is feasible since the

sample-and-hold control actions $h_{NL}(x(t_k))$, $h_{NL}(x(t_{k+1}))$, ... , $h_{NL}(x(t_{k+N-1}))$, which are based on the measured state $x(t_k)$ (Eq. 47c) at time t_k and the predicted states (Eq. 47b) at t_{k+1}, ... , t_{k+N-1}, maintain the process state within $\Omega_{\hat{\rho}_e}$ and meet the input constraints and Lyapunov-based constraints of Eqs. 47d–47e. For all $x(t_k) \in \Omega_{\hat{\rho}} \setminus \Omega_{\hat{\rho}_e}$, the controller $h_{NL}(x(t_k))$ is feasible by design since it is stabilizing in sample-and-hold with a sufficiently small sampling period and meets the constraints of Eqs. 47d and 47f. This shows that for all $x(0) \in \Omega_{\hat{\rho}}$, the LEMPC optimization problem of Eq. 47 will be recursively feasible if $x(t) \in \Omega_{\hat{\rho}}$ for all times.

Part 2. If $x(t_k) \in \Omega_{\hat{\rho}} \setminus \Omega_{\hat{\rho}_e}$, the LEMPC requires that the mode 2 constraint of Eq. 47f be satisfied, which leads to the following requirement for any solution requested by the LEMPC at time t_k

$$\begin{aligned}&\frac{\partial \hat{V}(x(t_k))}{\partial x}(Ax(t_k)+P_z(x(t_k))+Bu(t_k))\\ &\leq \frac{\partial \hat{V}(x(t_k))}{\partial x}(Ax(t_k)+P_z(x(t_k))+Bh_{NL}(x(t_k))) \leq -c_3|x(t_k)|^2\end{aligned} \tag{76}$$

Since Theorem 1 requires that Proposition 1 be met, Eq. 46 holds and

$$\frac{\partial \hat{V}(x(t_k))}{\partial x}\tilde{f}(x(t_k), h_{NL}(x(t_k)), 0) \leq -\hat{c}_3|x(t_k)|^2 \tag{77}$$

To account for the effect of disturbances, Eq. 77 can be used to bound the time-derivative of the Lyapunov function of the closed-loop system using the Lyapunov-based controller based on the empirical model for all $\tau \in [t_k, t_{k+1})$

$$\begin{aligned}\dot{\hat{V}}(x(\tau)) &= \frac{\partial \hat{V}(x(\tau))}{\partial x}\tilde{f}(x(\tau), h_{NL}(x(t_k)), w(\tau))\\ &\quad - \frac{\partial \hat{V}(x(t_k))}{\partial x}\tilde{f}(x(t_k), h_{NL}(x(t_k)), 0)\\ &\quad + \frac{\partial \hat{V}(x(t_k))}{\partial x}\tilde{f}(x(t_k), h_{NL}(x(t_k)), 0)\\ &\overset{(49),(77)}{\leq} L_x'|x(\tau)-x(t_k)|+L_w'|w(\tau)|-\hat{c}_3|x(t_k)|^2\\ &\leq -\frac{\hat{c}_3}{c_2}\hat{\rho}_e+L_x'|x(\tau)-x(t_k)|+L_w'|w(\tau)|\end{aligned} \tag{78}$$

where the final inequality results from Eq. 37a and the definition of the value of $\hat{V}(x)$ when $x(t_k) \in \Omega_{\hat{\rho}} \setminus \Omega_{\hat{\rho}_e}$. Using Eq. 50 and a derivation similar to that used to arrive at Eq. 69, we have

$$|x(\tau)-x(t_k)| \leq M\Delta \tag{79}$$

for all $\tau \in [t_k, t_{k+1}]$. Substituting this inequality and the bound θ on w into Eq. 78, and utilizing Eqs. 76 and 77, we have that the Lyapunov function of the closed-loop system under LEMPC mode 2 satisfies

$$\frac{\partial \hat{V}(x(\tau))}{\partial x}\tilde{f}(x(\tau), u(t_k), w(\tau)) \leq -\frac{\hat{c}_3}{c_2}\hat{\rho}_e+L_x'M\Delta+L_w'\theta \tag{80}$$

for all $\tau \in [t_k, t_{k+1})$. Substituting Eq. 74 into Eq. 80, integrating Eq. 80 over $\tau \in [t_k, t_{k+1}]$ and using continuity of the solution of Eq. 1 in a compact set, we have

$$\begin{aligned}\hat{V}(x(t_{k+1})) &\leq \hat{V}(x(t_k))-\epsilon_w,\\ \hat{V}(x(\tau)) &\leq \hat{V}(x(t_k)), \quad \forall\ \tau \in [t_k, t_{k+1}]\end{aligned} \tag{81}$$

This result shows that for all $x(t_k) \in \Omega_{\hat{\rho}} \setminus \Omega_{\hat{\rho}_e}$, the Lyapunov function of the closed-loop system under LEMPC mode 2 decreases throughout a sampling period, which means that the state will be driven back into $\Omega_{\hat{\rho}_e}$ in finite time.

When $x(t_k) \in \Omega_{\hat{\rho}_e}$, the predicted trajectory $\tilde{x}(t_{k+1}) \in \Omega_{\hat{\rho}_e}$ by Eq. 47e. By Propositions 2 and 3, the actual state $x(t_{k+1})$ is within a bound of the predicted state and the following holds

$$\begin{aligned}\hat{V}(x(t_{k+1})) &\leq \hat{V}(\tilde{x}(t_{k+1}))+f_V(|x(t_{k+1})-\tilde{x}(t_{k+1})|)\\ &\leq \hat{\rho}_e+f_V(f_w(\Delta))\end{aligned} \tag{82}$$

When Eq. 75 holds, Eq. 82 implies $x(t_{k+1}) \in \Omega_{\hat{\rho}}$. This completes the proof of Theorem 1 by showing that for any $x(0) \in \Omega_{\hat{\rho}}$, the closed-loop state trajectories of the actual process are maintained in $\Omega_{\hat{\rho}}$ provided that the assumptions of Theorem 1 are met.

Remark 6. *The stability discussion above shows that disturbances, which include plant-model mismatch, are required to be sufficiently small if closed-loop stability is to be maintained under LEMPC. It may in general be difficult to identify an empirical model for use in LEMPC for which the plant-model mismatch is low over a large enough operating range that the stability region for use in LEMPC is not restrictively small, since a small stability region would likely not perform much differently than steady-state operation. One method for improving the range over which an empirical model is applicable (and thus possibly increasing the size of $\Omega_{\hat{\rho}}$) is to use higher-order polynomials in the PNLSS identification. This concept is demonstrated in the chemical process example of this work.*

Remark 7. *For the reasons noted in Remark 3 of* Ref. 55*, a longer prediction horizon may not be able to improve the closed-loop performance of an EMPC formulated with an empirical model, especially if there are significant differences between the actual process behavior and that predicted by the model.*

Remark 8. *For systems that can be approximated over the region of interest with low-order polynomials (e.g., second or third order), a significant benefit in terms of computation time may be observed when using the low-order empirical model as compared with using the full nonlinear first-principles process model. An example is given for which this is the case in the "Application of LEMPC Based on the Well-Conditioned PNLSS Model to the Chemical Process" section of this article. If computation time is a significant consideration for an actual process control system, an empirical model may be considered even if a first-principles model can be derived for a given process.*

Remark 9. *One major factor in the stability of the LEMPC of* Eq. 47 *is that it is a feedback control strategy, incorporating a measurement of the actual process state at every sampling period so that it is able to tolerate some level of process disturbances and plant-model mismatch.*

Remark 10. *The feasibility and speed of convergence of the LEMPC optimization problem depend on the choice of the Lyapunov function and the stability region used in the optimization problem; however, the effect of the Lyapunov function and the stability region cannot in general be characterized a priori but such a characterization can be obtained through numerical simulations using different Lyapunov functions to determine how the choice of the parameters of the P matrix (when a quadratic Lyapunov function*

$V(x) = x^T P x$ *is used) and of the size of the level set influence the aforementioned LEMPC characteristics.*

Application of LEMPC Based on the Well-Conditioned PNLSS Model to the Chemical Process

In the following sections, we return to the CSTR example described above and compare the closed-loop state and input trajectories for the CSTR under the LEMPC utilizing the first-principles model of Eq. 10 and the LEMPC utilizing the empirical model of Eq. 27 developed using PNLSS with numerical stability constraints. In addition, comparisons will be made between the results of using the nonlinear empirical model of Eq. 27 in LEMPC with the results of using the linear empirical models described in Ref. 55 with LEMPC. The process model used here is the same as that in Ref. 55 to facilitate direct comparison.

As noted previously, it is assumed that the dynamics of the CSTR are perfectly modeled by Eq. 10, and that the available control actions are constrained by the actuators to the sets in Eq. 14. Simulations assuming full state feedback were used to perform system identification using PNLSS per the optimization problem of Eq. 26 to develop the nonlinear empirical model of Eq. 27, where u and x are written in terms of deviation variables as defined in Eqs. 12 and 13. It is desired to produce the maximum amount of B possible in a given time period while maintaining the states within a compact region of state-space containing the steady-state $[C_{As}\ \ T_s] = [1.2\ \text{kmol/m}^3\ \ 438.0\ \text{K}]$. Thus, the cost function $\bar{L}_e$ to be used in the LEMPC of Eq. 47 is the negative of the time-average of the total amount of B produced per the Arrhenius rate law throughout a time period (it is the negative since Eq. 47 is a minimization problem and our goal is to maximize the production of B)

$$\bar{L}_e(x,u) = -\frac{1}{(t_{k+N}-t_k)}\int_{t_k}^{t_{k+N}} k_0 e^{-E/RT(\tau)} C_A^2(\tau)\ d\tau \tag{83}$$

In addition to the bounds on the control actions caused by the actuators, we assume that the amount of reactant that is available to be fed to the reactor is limited in a given time period $t_p = 1.0$ h by the following constraint:

$$\frac{1}{t_p}\int_0^{t_p} u_1(\tau)\ d\tau = 0.0\,\text{kmol/m}^3 \tag{84}$$

To maintain process stability when the empirical process model of Eq. 27 is used, the Lyapunov stability region constraints for LEMPC must be defined. The stability region is defined using a Lyapunov-based controller $h(x) = [h_1(x)\ \ h_2(x)]^T$ for the process that meets the requirements of Eq. 37. The Lyapunov-based controller is developed here by considering h_1 and h_2 separately. To ensure that the material constraint of Eq. 84 is satisfied by the closed-loop process under controller $h(x)$, the value of h_1 is set to 0.0 $kmol/m^3$. The value of h_2 is determined using a Lyapunov-based control law calculated based on the process model. It is assumed here, as would be the case in practice, that the only process model available from which to determine $h_2(x)$ is the empirical model of Eq. 27. To develop the control law, terms in the empirical model of Eq. 3 are denoted as functions $f : R^n \to R^n$ and $g : R^n \to R^n \times R^m$ as follows

$$\dot{x} = \underbrace{Ax + P_z(x)}_{=:f(x)} + \underbrace{B}_{=:g(x)}\, u \tag{85}$$

As there are two inputs for this chemical process example, $g(x) = [g_1\ \ g_2]$ where $g_1, g_2 \in R^n$. The control law for h_2 is then determined from the Lyapunov-based control law in Ref. 57

$$h_2(x) = \begin{cases} -\dfrac{L_f\hat{V} + \sqrt{L_f\hat{V}^2 + L_{g_2}\hat{V}^4}}{L_{g_2}\hat{V}}, & \text{if } L_{g_2}\hat{V} \neq 0 \\ 0, & \text{if } L_{g_2}\hat{V} = 0 \end{cases} \tag{86}$$

where $L_f\hat{V}$ and $L_{g_2}\hat{V}$ denote the Lie derivatives of the Lyapunov function $\hat{V}(x)$ with respect to the vector fields $f(x)$ and $g_2(x)$. The Lyapunov function $\hat{V}$ was chosen as $\hat{V}(x) = x^T P x$ with P being the following positive definite matrix

$$P = \begin{bmatrix} 1030 & 20 \\ 20 & 0.6 \end{bmatrix} \tag{87}$$

Extensive simulations were performed using the controller $h(x)$ in closed-loop with the empirical model of Eq. 27 to obtain an estimate of the stability region of the actual process. Because an estimate of the process model was used to determine the stability region, a conservative subset of this stability region was chosen for the LEMPC design. This subset was chosen based on simulations that showed it was a region within which the first-principles and empirical models show good agreement of the state trajectories, but was large enough that there was a significant benefit with LEMPC operation compared with steady-state operation. The stability regions for use in the Lyapunov-based constraints of Eqs. 47e–47f were taken to be $\Omega_{\hat{\rho}}$ with $\hat{\rho} = 370$ and $\Omega_{\hat{\rho}_e}$ with $\hat{\rho}_e = 350$.

Using the above constraints, two different LEMPCs will be compared, each with the general form of Eq. 47 and formulated for use in closed-loop with the process model of Eq. 10. Both LEMPCs use the cost function of Eq. 83, the input constraints of Eq. 14 and Eq. 84, $\hat{\rho}_e = 350$, an integration step size of 10^{-4} h with the Explicit Euler numerical integration method, a sampling period $\Delta = 0.01$ h, and a prediction horizon $N = 10$. The first of the LEMPCs, which will henceforth be designated as the second-order empirical LEMPC, uses the PNLSS dynamic model of Eq. 27. The second of the LEMPCs, which will henceforth be designated as the first-principles LEMPC, uses the nonlinear dynamic model of Eq. 10. Because it is assumed that the nominal model of Eq. 10 perfectly represents the process dynamics, the mode 2 constraint of Eq. 47f was not used in this first-principles LEMPC since there is no measurement noise or plant-model mismatch to drive the state outside of $\Omega_{\hat{\rho}_e}$. For both LEMPCs, the material constraint of Eq. 84 is applied in the manner outlined in Ref. 12. The first-principles and second-order empirical LEMPC optimization problems were solved at each sampling time using Ipopt. To account for practical implementation considerations, the optimizations were terminated and the current estimate of the optimization variable u was returned if they were not complete at the end of a sampling period. The actuator dynamics were considered to be sufficiently fast such that the returned solutions were directly implemented on the process of Eq. 10 with a zero-order hold of length Δ.

Empirical LEMPC compared with first-principles LEMPC

The process of Eq. 10 was simulated in closed-loop with both the second-order empirical and the first-principles LEMPCs for one operating period of length $t_p = 1$ h. The resulting state and input trajectories are shown in Figure 6.

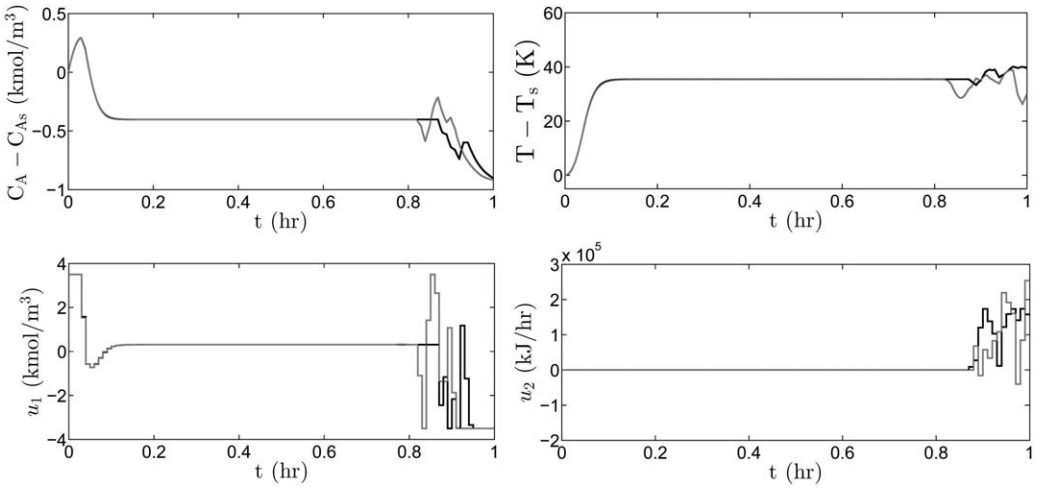

Figure 6. Trajectories of the states and inputs for the Eq. 10 CSTR model throughout one operating period $t_p = 1$ h when controlled by the first-principles LEMPC (black trajectories) and the second-order empirical LEMPC (gray trajectories) starting from C_{As}, T_s.

These trajectories exhibit behavior similar to that reported in Ref. 55. The state trajectories are initiated from the steady-state $[C_{As}\ T_s] = [1.2\ \text{kmol/m}^3\ 438.0\ \text{K}]$, and they subsequently level off at a new steady-state on the boundary of the stability region with a temperature greater than that at the initial steady-state since the production rate of B increases with increasing temperature. The concentration of A in the reactor decreases at the end of the simulation as the inlet concentration of A is reduced to meet the material constraint of Eq. 84. The decrease in C_A allows the reactor temperature to increase to enhance generation of B without leaving the stability region. Figure 6 shows that the state and input trajectories using the second-order empirical LEMPC closely track those of the first-principles LEMPC until approximately 0.8 h, at which time the first-principles and second-order empirical LEMPCs request significantly different control actions because they require that the material constraint be met in the short remainder of the operating interval though different process models are being used in the LEMPCs to ensure that the predicted trajectories meet this constraint. The differences in the requested control actions cause the process states under the second-order empirical LEMPC to leave $\Omega_{\hat{\rho}_e}$ six times at the end of the operating period, starting at approximately 0.85 h, while the first-principles LEMPC never leaves $\Omega_{\hat{\rho}_e}$. This means that in addition to the differences in the process state trajectories that result from using different model equations to satisfy constraints, there are added differences that result because the second-order empirical LEMPC switches to mode 2 operation though the first-principles LEMPC remains operating in mode 1. Figure 7 illustrates the state-space behavior of the first-principles and second-order empirical LEMPCs, including their initial close agreement, their evolution along the edge of the stability region between approximately $t = 0.1$ and 0.8 h, and their subsequent deviation from one another. Despite the differences at the end of the interval, the overall closeness of the state and input trajectories using both the second-order empirical and first-principles LEMPCs shows that the second-order empirical LEMPC using the model derived from PNLSS with numerical stability constraints may be suitable for the process in this example and has the potential to produce similarly good results for other processes.

The main reason for considering the first-principles LEMPC over the second-order empirical LEMPC, since both maintain process stability within the stability region, would be related to the economic benefit of using the first-principles LEMPC. Since the first-principles LEMPC represents the ideal case in which the full nonlinear process model is known so that the profit of the actual process is being maximized, it would be expected to have a higher profit than any variants of that LEMPC. In order to quantify the closed-loop performance of the first-principles LEMPC and compare it with that of the second-order empirical LEMPC, the following average economic cost index is used (which has units kmol/m^3)

$$J_e = \frac{1}{t_f}\int_0^{t_f} k_0 e^{-E/RT(t)} C_A^2(t)\ dt \tag{88}$$

where t_f is the length of time for which the closed-loop process is simulated. This average economic cost represents the time-average rate of generation of B throughout process operation

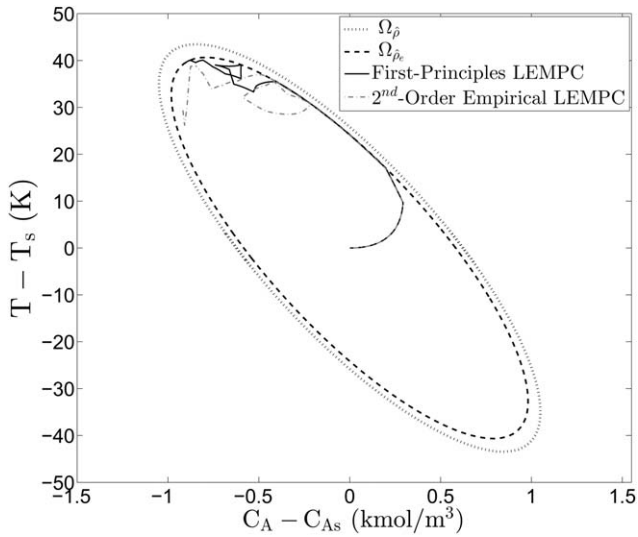

Figure 7. State-space representation of closed-loop state trajectories for one operating period $t_p = 1$ h for the Eq. 10 CSTR model under the first-principles LEMPC (solid trajectory) and the second-order empirical LEMPC (dashed-dotted trajectory) starting from C_{As}, T_s.

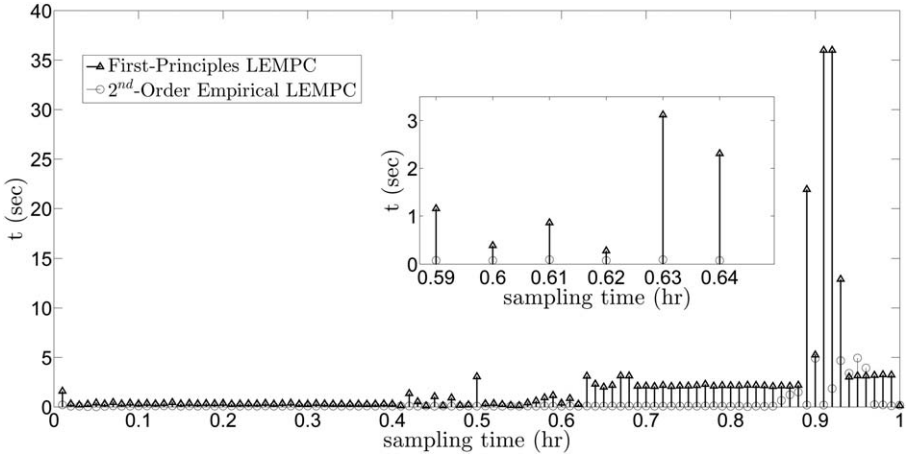

Figure 8. Chart showing, for each sampling period, the computation time used for the optimization problems of the first-principles LEMPC (triangle markers) and the second-order empirical LEMPC (circle markers) during one operating period.

and thus reflects the profit of the process (i.e., higher J_e implies better process closed-loop performance). For the closed-loop CSTR under the second-order empirical LEMPC, J_e is 16.1227, while for the first-principles LEMPC it is 16.1626. This shows that for an operating period of 1 h, an improvement of less than 0.3% is achieved when using the first-principles LEMPC instead of the second-order empirical LEMPC.

One major benefit of using the second-order empirical state-space model of Eq. 27 compared to the full process model of Eq. 10 is the reduction in computation time required by the LEMPC with the simpler empirical model. Figure 8 shows the amount of time in CPU seconds to find a solution to the first-principles and second-order empirical LEMPCs for each sampling period. The optimization problems take longer to solve at the end of the one hour simulation for both LEMPCs due to the increased number of function evaluations required to ensure that the material constraint is satisfied in the small remaining time of operation while the other input and stability region constraints remain satisfied (the computation time is increased as there are less degrees of freedom when finding a solution). As demonstrated in Figure 8, the first-principles LEMPC optimization problem terminated early two times in the operating period because it reached the end of the 0.01 h (36 s) sampling period before finding a solution (and thus returned a suboptimal solution). The second-order empirical LEMPC, however, never came close to the 36 s computation time constraint, and the optimal solutions were obtained in less than 0.15 s in most of the sampling periods. The sum of the computation times for all sampling periods in the operating window (total computation time) was 206.317 s for the first-principles LEMPC, but only 30.108 s for the second-order empirical LEMPC. The first-principles LEMPC is much more computationally expensive than the second-order empirical LEMPC, with a total computation time that is 580% higher than for the second-order empirical LEMPC.

To investigate the long-term performance and computation time differences between the first-principles and second-order empirical LEMPCs, a ten-hour simulation was conducted for the CSTR of Eq. 10, and the results are shown in Figures 9–12. The average economic cost per Eq. 88 was 15.91 for the second-order empirical LEMPC and 15.96 for the first-principles LEMPC; less than 0.4% performance improvement is observed when using the first-principles LEMPC. Both the first-principles and the second-order empirical LEMPCs significantly outperform steady-state operation; the average economic cost at the end of the 10 h is 13.88 for steady-state operation at $[C_{As}\ T_s\ C_{A0s}\ Q_s]$. Thus, operating the process of Eq. 10 under the second-order empirical LEMPC is 14.6% more profitable than operating it at steady-state.

The computation times for the first-principles and second-order empirical LEMPCs were also compared for the ten-hour simulation. The average total computation time for each 1 h operating period of the ten-hour simulation is 197.682 s for the first-principles LEMPC and 26.229 s for the second-order empirical LEMPC. The first-principles LEMPC average computation time is 650% higher than that of the second-order empirical LEMPC.

The results using the second-order empirical LEMPC above can be compared to the results presented for the linear empirical model in the chemical process example in Ref. 55. The linear empirical model of Eqs. 57 and 58 in Ref. 55 is henceforth

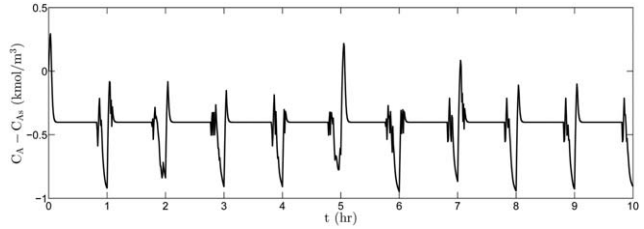

Figure 9. Trajectory of the CSTR concentration over 10 h for the CSTR model of Eq. 10 under the second-order empirical LEMPC.

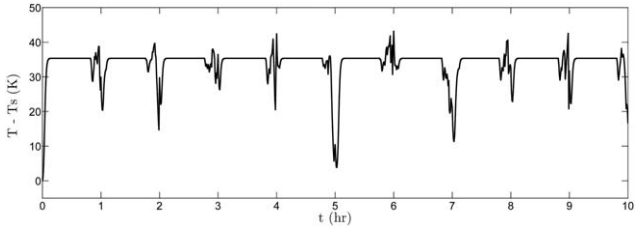

Figure 10. Trajectory of the CSTR temperature over 10 h for the CSTR model of Eq. 10 under the second-order empirical LEMPC.

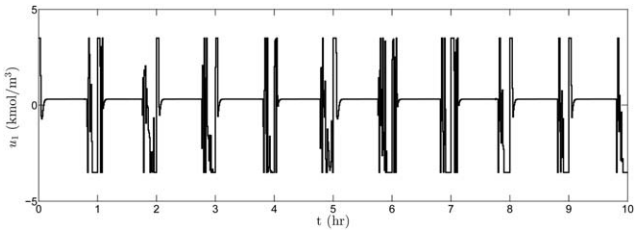

Figure 11. Trajectory of the feed concentration input to the CSTR over 10 h for the CSTR model of Eq. 10 under the second-order empirical LEMPC.

referred to as the linear model. Because the second-order empirical model of Eq. 27 is a better approximation of the actual system than a linear model, the LEMPC using the second-order empirical model calculates inputs that do not cause the closed-loop state trajectories to leave the set $\Omega_{\hat{\rho}_e}$ as often as do the trajectories from using the linear model. A comparison of Figure 4 of Ref. 55 for the linear model with Figure 6 for the second-order empirical model demonstrates this. From these figures, it is seen that the u_1 and hence C_A trajectories for the linear model exhibit extensive chattering caused by frequent switching of the LEMPC between mode 1 and 2 operation; this chattering is not exhibited in the trajectories resulting from the use of the second-order empirical model, and as previously noted, the second-order empirical model only switched between mode 1 and mode 2 operation six times. Another result of using the second-order empirical model as a better approximation of the actual process system is that the stability region used with the second-order empirical model is significantly larger than with the linear empirical model (for the linear model, $\hat{\rho}_e$ is 55.0, while for the second-order empirical model, it is 350). The more restricted stability region results in a lesser value of J_e after an hour of simulation for the linear model than for the second-order empirical model, since the state variables cannot extend as far to maximize the profit during the part of the trajectory when they remain on the edge of the stability region (compare, for example, the temperature of approximately 20 K in the time period from 0.2 to 0.8 h in Figure 4 of Ref. 55 with the temperature of approximately 35 K in Figure 6). Over one operating period of 1 h, the average economic cost index of the second-order empirical LEMPC is approximately 2.7% greater using the second-order empirical model than the linear model, and for the ten-hour simulation, it is approximately 4.1% greater using the second-order empirical model than the linear model. The computation time for the linear LEMPC is less than that for the second-order empirical LEMPC, however. The total computation time for one operating period is 36.9% greater for the second-order empirical LEMPC than for the linear LEMPC, and the average total computation time for a one-hour operating period from the ten-hour simulation is 11.1% greater for the second-order empirical LEMPC than for the linear LEMPC. Both the second-order empirical and linear LEMPCs have profits close to those of the LEMPCs for the actual process with the corresponding stability region (the profit from the second-order empirical LEMPC is close to that of the first-principles LEMPC, and the profit from the linear LEMPC is close to that of the actual process with which it is compared in Ref. 55), and both have computation times much lower than those for the actual process with the corresponding stability region. Thus, the decision to use the linear, second-order empirical, or first-principles LEMPC for this process would depend on the practical significance of a percentage change in profit compared to a percentage change in computation time.

Remark 11. *The simulation results in this section demonstrate that for the given chemical process example, the proposed approach using the LEMPC incorporating a nonlinear empirical model is robust to the mismatch between the nonlinear empirical model and the first-principles model because the LEMPC with the empirical model maintains process stability and good performance.*

Improved accuracy with higher-order empirical models

In the comparison between the second-order empirical and first-principles LEMPCs above, it was noted that the first-principles LEMPC had a greater profit than the second-order empirical LEMPC, since the first-principles LEMPC was taken to represent the actual process and the second-order empirical LEMPC was only an approximation. It would thus be expected that as the accuracy of the model derived from the PNLSS model identification procedure is increased (additional nonlinear terms are kept in the function $P_z(x)$ of Eq. 3) that the resulting model would more accurately represent the actual process dynamics over a larger region and thus allow a greater profit for the process, closer to that which could be achieved with the LEMPC using the actual first-principles process model of Eq. 10. This motivated the identification of an empirical model using higher-order terms for use in LEMPC, which will be described in this section.

To determine the effect of using an empirical model using higher-order nonlinear terms on the performance and computation time of an LEMPC, the PNLSS model identification procedure of Eq. 26 was used to find empirical process models with both a third-order polynomial and a fourth-order polynomial for $P_z(x)$ that satisfy the numerical stability constraints. Extensive simulations were used to validate the third and fourth-order models obtained. Because all coefficients of the fourth-order terms from the verified fourth-order model were very small (on the order of 10^{-13}), the third-order model was considered to be sufficient to demonstrate the impact of the higher-order terms on the LEMPC output, so that was the only model for which closed-loop LEMPC simulations were conducted. The validated third-order model is

$$\begin{aligned}\frac{dx_1}{dt} = &-34x_1 - 0.495x_2 + 48x_1^2 + 1.95x_1x_2 \\ &+ 18x_2^2 - 92x_1^3 - 0.000707x_1^2x_2 \\ &- 0.000016x_1x_2^2 - 0.0005x_2^3 - 4.6u_1 - 0.000008u_2\end{aligned} \tag{89a}$$

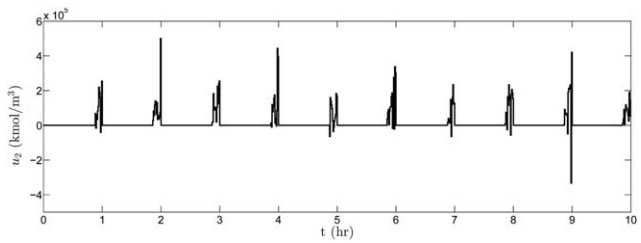

Figure 12. Trajectory of the heat input to the CSTR over 10 h for the CSTR model of Eq. 10 under the second-order empirical LEMPC.

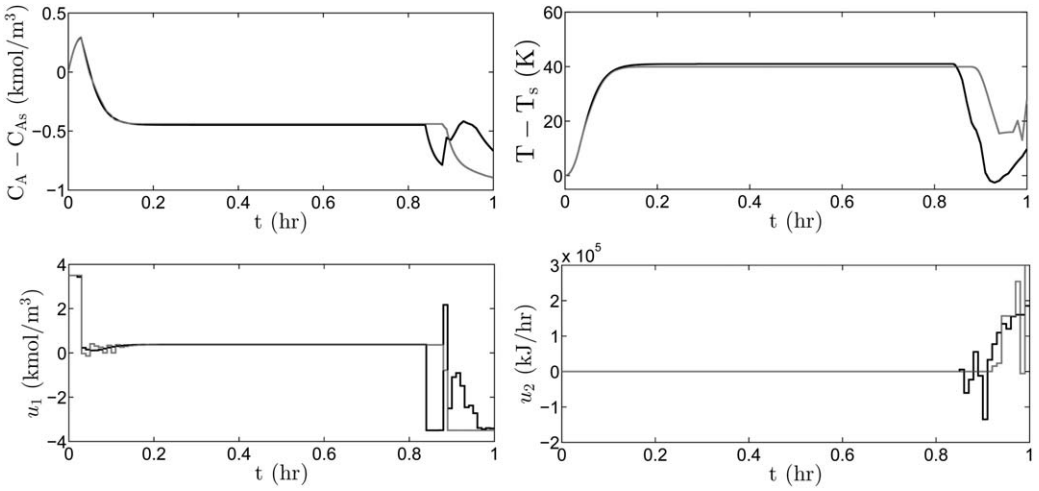

Figure 13. Trajectories of the states and inputs for the Eq. 10 CSTR model throughout one operating period $t_p = 1$ h when controlled by the first-principles LEMPC (black trajectories) and the third-order empirical LEMPC (gray trajectories) starting from C_{As}, T_s.

$$\begin{aligned}\frac{dx_2}{dt} &= 1436x_1 + 18x_2 - 1475x_1^2 - 51x_1x_2 \\ &\quad -0.00509x_2^2 - 0.0005x_1^3 - 0.0233x_1^2x_2 \\ &\quad -0.000526x_1x_2^2 - 0.000024x_2^3 - 11u_1 + 0.00567u_2\end{aligned} \tag{89b}$$

To use this third-order model in the LEMPC of Eq. 47, it is necessary to first specify the stability region for the Lyapunov-based constraints of Eqs. 47e–47f. The Lyapunov function for this third-order process model, in closed-loop with a Lyapunov-based controller $h(x)$ designed similarly to that used for the second-order empirical LEMPC ($h(x) = [0\, h_2(x)]^T$ where $h_2(x)$ is designed using Eq. 86 with the third-order model), was again taken to have the form $\hat{V}(x) = x^T P x$, but with P as

$$P = \begin{bmatrix} 1170 & 24 \\ 24 & 0.56 \end{bmatrix} \tag{90}$$

After extensive closed-loop simulations, the stability region for LEMPC including the third-order empirical model was taken to be $\Omega_{\hat{\rho}}$ with $\hat{\rho} = 485$ and $\Omega_{\hat{\rho}_e}$ with $\hat{\rho}_e = 285$.

As was done for the second-order empirical LEMPC, two different LEMPCs will now be compared. Each has the general form of Eq. 47 and is formulated for use in closed-loop with the process of Eq. 10; however, the first LEMPC (which will be referred to as the third-order empirical LEMPC) uses the third-order PNLSS model of Eq. 89 while the second LEMPC (which will be referred to as the first-principles LEMPC) uses the dynamic model of Eq. 10. Both LEMPCs define the stability region using $\hat{\rho}_e = 285$; the first-principles LEMPC does not require mode 2 operation, though the third-order empirical LEMPC requires both mode 1 and mode 2 operation. As in the example presented above, these LEMPCs use the cost function of Eq. 83, the input constraints of Eq. 14 and Eq. 84, an Explicit Euler integration step size of $h_c = 10^{-4}$ h, $\Delta = 0.01$ h, $t_p = 1$ h, and $N = 10$, and also terminate the optimization problem after 0.01 h has elapsed. The closed-loop state and input trajectories for one hour of operation for these two LEMPCs are presented in Figure 13, with the state-space representation of these trajectories in Figure 14.

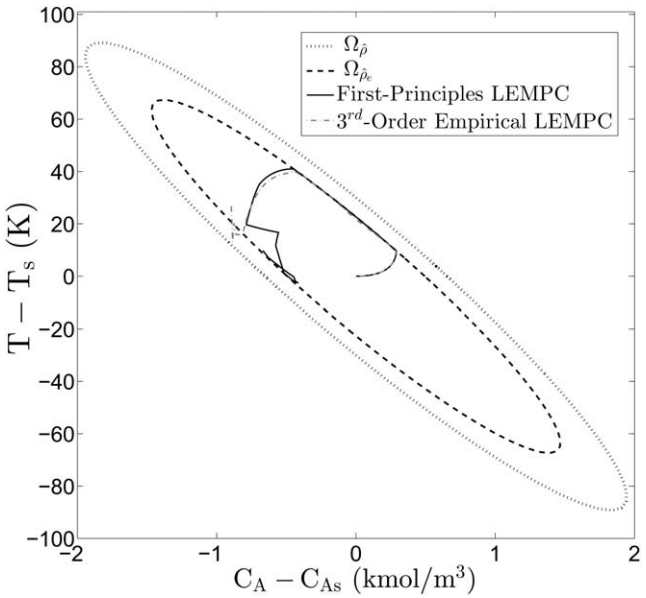

Figure 14. State-space representation of closed-loop state trajectories for one operating period $t_p = 1$ h for the Eq. 10 CSTR model under the first-principles LEMPC (solid trajectory) and the third-order empirical LEMPC (dashed-dotted trajectory) starting from C_{As}, T_s.

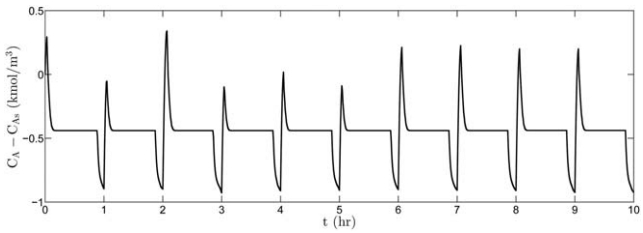

Figure 15. Trajectory of the CSTR concentration over 10 h for the CSTR model of Eq. 10 under the third-order empirical LEMPC.

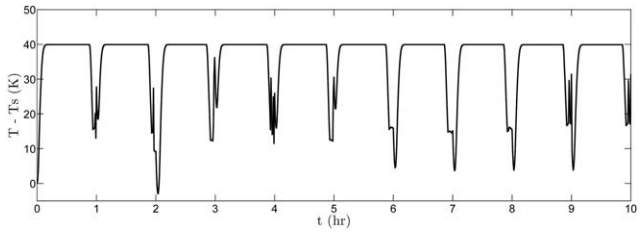

Figure 16. Trajectory of the CSTR temperature over 10 h for the CSTR model of Eq. 10 under the third-order empirical LEMPC.

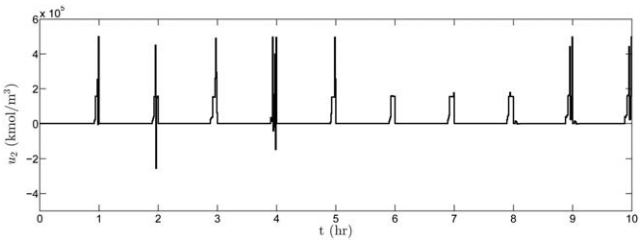

Figure 18. Trajectory of the heat input to the CSTR over 10 h for the CSTR model of Eq. 10 under the third-order empirical LEMPC.

The trajectories in Figure 13 show similar behavior to those in Figure 6, with a notable difference being that the temperature is able to reach a higher value during the period of time from approximately $t = 0.1$ to 0.8 h in the third-order case of Figure 13 due to the different stability region calculated for the more accurate third-order model. In addition, the stability region difference contributes to the fact that both the third-order empirical and first-principles LEMPCs produce a drop in reactor temperature at the end of the hour simulation where the material constraints come in to play, whereas the temperatures increase at the end of this period for the second-order case.

A ten-hour simulation was also conducted for the third-order empirical LEMPC, and the resulting state and input trajectories are shown in Figures 15–18. The average value of the economic cost index in one operating period throughout this ten-hour simulation was 16.26, which is 17% greater than steady-state operation (for which the average economic cost index for one operating period is 13.88). This is a greater performance enhancement over steady-state operation than was attained with the second-order empirical LEMPC of the previous section.

To facilitate a comparison between the third-order empirical and first-principles LEMPCs from this section with the second-order empirical and first-principles LEMPCs from the previous section, we will identify the first-principles LEMPC from the previous section as the First-Principles 1 LEMPC and the first-principles LEMPC from this section as the First-Principles 2 LEMPC. The average economic cost index of Eq. 88 over one hour of operation and the total computation time for one hour of operation are shown in Table 2 for the empirical and first-principles models of this section and of the previous section. It is notable that the average economic cost index for the third-order empirical LEMPC and the First-Principles 2 LEMPC are higher than for the two LEMPCs of the previous section due to the different stability region chosen for the more accurate third-order empirical model. It is also notable that the performance gap between the third-order empirical LEMPC and the First-Principles 2 LEMPC is less than that between the second-order empirical LEMPC and the First-Principles 1 LEMPC since the third-order empirical model more accurately captures the dynamics of the first-principles model (the performance of the First-Principles 2 LEMPC is only 0.09% higher than that of the third-order empirical LEMPC, while the performance of the First-Principles 1 LEMPC was about 0.3% higher than that of the second-order empirical LEMPC). It would be expected, however, that the computation time would increase as the polynomial approximation of the process dynamics contains more terms to evaluate; Table 2 shows that the total computation time for the third-order empirical LEMPC for one operating period is 116% greater than that of the second-order empirical LEMPC.

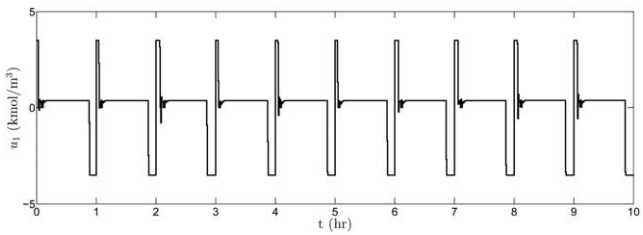

Figure 17. Trajectory of the feed concentration input to the CSTR over 10 h for the CSTR model of Eq. 10 under the third-order empirical LEMPC.

Conclusions

In this work, a nonlinear system identification technique was developed for general nonlinear systems with affine inputs using a PNLSS model with additional constraints on the numerical stability of the identified model so that the identification process produces empirical models that can be numerically integrated with explicit methods without using a very small integration step size. The motivation for this is that such models have an advantage in MPC applications, in contrast to the models identified with standard techniques that may require a step size too small for real-time use. This work demonstrates the benefits of the proposed system identification method in MPC by developing the formulation of an LEMPC scheme that uses an empirical model derived from the PNLSS method accounting for model well-conditioning to predict the process dynamics. A stability analysis of the closed-loop system under this controller showed that it can stabilize the closed-loop process dynamics by confining the states to a compact region of state-space when certain conditions are met. A chemical process example demonstrated that incorporating the well-conditioned empirical model in place of a first-principles model in LEMPC has significant computational advantages

Table 2. Comparison of Average Economic Cost (J_e) and Total Computation Time for One Operating Period (1 h) Using Various LEMPCs

Model	J_e	Computation Time (s)
Second-order empirical	16.1227	30.108
Third-order empirical	16.7569	65.156
First-Principles 1	16.1626	206.317
First-Principles 2	16.7712	201.428

such that the LEMPC with the empirical model can be used for real-time control, with minimal reduction in profit compared with using the first-principles model.

Acknowledgment

Financial support from the National Science Foundation and the Department of Energy is gratefully acknowledged.

Literature Cited

1. Rawlings JB, Angeli D, Bates CN. Fundamentals of economic model predictive control. In: *Proceedings of the 51st IEEE Conference on Decision and Control*. Maui, HI, 2012;3851–3861.
2. Heidarinejad M, Liu J, Christofides PD. Economic model predictive control of nonlinear process systems using Lyapunov techniques. *AIChE J*. 2012;58:855–870.
3. Müller MA, Angeli D, Allgöwer F. On convergence of averagely constrained economic MPC and necessity of dissipativity for optimal steady-state operation. In: *Proceedings of the American Control Conference*. Washington, DC, 2013;3141–3146.
4. Grüne L, Stieler M. Asymptotic stability and transient optimality of economic MPC without terminal conditions. *J Process Control*. 2014;24:1187–1196.
5. Ellis M, Christofides PD. On finite-time and infinite-time cost improvement of economic model predictive control for nonlinear systems. *Automatica*. 2014;50:2561–2569.
6. Amrit R, Rawlings JB, Angeli D. Economic optimization using model predictive control with a terminal cost. *Annu Rev Control*. 2011;35:178–186.
7. Huang R, Biegler LT, Harinath E. Robust stability of economically oriented infinite horizon NMPC that include cyclic processes. *J Process Control*. 2012;22:51–59.
8. Diehl M, Amrit R, Rawlings JB. A Lyapunov function for economic optimizing model predictive control. *IEEE Trans Automat Control*. 2011;56:703–707.
9. Zhang J, Liu S, Liu J. Economic model predictive control with triggered evaluations: state and output feedback. *J Process Control*. 2014;24:1197–1206.
10. Ellis M, Christofides PD. Optimal time-varying operation of nonlinear process systems with economic model predictive control. *Ind Eng Chem Res*. 2014;53:4991–5001.
11. Ellis M, Christofides PD. Real-time economic model predictive control of nonlinear process systems. *AIChE J*. 2015;61:555–571.
12. Ellis M, Durand H, Christofides PD. A tutorial review of economic model predictive control methods. *J Process Control*. 2014;24:1156–1178.
13. Verhaegen M, Deprettere E. A fast, recursive MIMO state space model identification algorithm. In: *Proceedings of the 30th IEEE Conference on Decision and Control*. Brighton, UK, 1991;1349–1354.
14. Larimore WE. Canonical variate analysis in identification, filtering, and adaptive control. In: *Proceedings of the 29th IEEE Conference on Decision and Control*. Honolulu, HI, 1990;596–604.
15. Van Overschee P, De Moor B. N4SID: Subspace algorithms for the identification of combined deterministic-stochastic systems. *Automatica*. 1994;30:75–93.
16. Doyle FJ, Pearson RK, Ogunnaike BA. *Identification and Control Using Volterra Models*. London: Springer, 2002.
17. Patrikar A, Provence J. Nonlinear system identification and adaptive control using polynomial networks. *Math Comput Model*. 1996;23:159–173.
18. Paduart J, Lauwers L, Swevers J, Smolders K, Schoukens J, Pintelon R. Identification of nonlinear systems using polynomial nonlinear state space models. *Automatica*. 2010;46:647–656.
19. Fruzzetti KP, Palazoğlu A, McDonald KA. Nonlinear model predictive control using Hammerstein models. *J Process Control*. 1997;7:31–41.
20. Sriniwas GR, Arkun Y. A global solution to the nonlinear model predictive control algorithms using polynomial ARX models. *Comput Chem Eng*. 1997;21:431–439.
21. Billings SA. *Nonlinear System Identification: NARMAX Methods in the Time, Frequency, and Spatio-Temporal Domains*. Wiley, 2013.
22. Patwardhan RS, Lakshminarayanan S, Shah SL. Constrained nonlinear MPC using Hammerstein and Wiener models: PLS framework. *AIChE J*. 1998;44:1611–1622.
23. Norquay SJ, Palazoglu A, Romagnoli JA. Model predictive control based on Wiener models. *Chem Eng Sci*. 1998;53:75–84.
24. Bloemen HHJ, Van Den Boom TJJ, Verbruggen HB. Model-based predictive control for Hammerstein-Wiener systems. *Int J Control*. 2001;74:482–495.
25. Aumi S, Mhaskar P. Integrating data-based modeling and nonlinear control tools for batch process control. *AIChE J*. 2012;58:2105–2119.
26. Ławryńczuk M. Practical nonlinear predictive control algorithms for neural Wiener models. *J Process Control*. 2013;23:696–714.
27. Akpan VA, Hassapis GD. Nonlinear model identification and adaptive model predictive control using neural networks. *ISA Trans*. 2011;50:177–194.
28. Ławryńczuk M. Computationally efficient nonlinear predictive control based on neural Wiener models. *Neurocomputing*. 2010;74:401–417.
29. Chou CT, Verhaegen M. Subspace algorithms for the identification of multivariable dynamic errors-in-variables models. *Automatica*. 1997;33:1857–1869.
30. Van Overschee P, De Moor B. *Subspace Identification for Linear Systems: Theory, Implementation, Application*. Boston, MA: Kluwer Academic Publishers, 1996.
31. Verhaegen M, Dewilde P. Subspace model identification Part 1. The output-error state-space model identification class of algorithms. *Int J Control*. 1992;56:1187–1210.
32. Viberg M. Subspace-based methods for the identification of linear time-invariant systems. *Automatica*. 1995;31:1835–1851.
33. Qin SJ. An overview of subspace identification. *Comput Chem Eng*. 2006;30:1502–1513.
34. Huang B, Kadali R. Dynamic modeling, predictive control and performance monitoring. London: Springer, 2008.
35. Mardi NA, Wang L. Subspace-based model predictive control of time-varying systems. In: *Proceedings of the 48th IEEE Conference on Decision and Control, held jointly with the 28th Chinese Control Conference*. Shanghai, China, 2009;4005–4010.
36. Favoreel W, De Moor B, Van Overschee P. Subspace state space system identification for industrial processes. *J Process Control*. 2000;10:149–155.
37. Pence BL, Fathy HK, Stein JL. Recursive maximum likelihood parameter estimation for state space systems using polynomial chaos theory. *Automatica*. 2011;47:2420–2424.
38. Schön TB, Wills A, Ninness B. System identification of nonlinear state-space models. *Automatica*. 2011;47:39–49.
39. Lapin SV. Identification of time-varying nonlinear systems using Chebyshev polynomials. *J Comput Appl Math*. 1993;49:121–126.
40. Liu GP, Kadirkamanathan V, Billings SA. On-line identification of nonlinear systems using Volterra polynomial basis function neural networks. *Neural Networks*. 1998;11:1645–1657.
41. Mahmoodi S, Poshtan J, Jahed-Motlagh MR, Montazeri A. Nonlinear model predictive control of a pH neutralization process based on Wiener–Laguerre model. *Chem Eng J*. 2009;146:328–337.
42. Marconato A, Sjöberg J, Schoukens J. Initialization of nonlinear state-space models applied to the Wiener–Hammerstein benchmark. *Control Eng Pract*. 2012;20:1126–1132.
43. Widanage WD, Stoev J, Van Mulders A, Schoukens J, Pinte G. Nonlinear system-identification of the filling phase of a wet-clutch system. *Control Eng Pract*. 2011;19:1506–1516.
44. Dutta A, Zhong Y, Depraetere B, Van Vaerenbergh K, Ionescu C, Wyns B, Pinte G, Nowe A, Swevers J, De Keyser R. Model-based and model-free learning strategies for wet clutch control. *Mechatronics*. 2014;24:1008–1020.
45. Paduart J, Lauwers L, Pintelon R, Schoukens J. Identification of a Wiener–Hammerstein system using the polynomial nonlinear state space approach. *Control Eng Pract*. 2012;20:1133–1139.
46. Van Mulders A, Schoukens J, Volckaert M, Diehl M. Two nonlinear optimization methods for black box identification compared. *Automatica*. 2010;46:1675–1681.
47. Harnack G, Lauwers L, Pintelon R, Schoukens J. Identification of nonlinear feedback systems using a structured polynomial nonlinear state space model. In: *Proceedings of the 15th IFAC Symposium on System Identification*, Vol. 15. Saint-Malo, France, 2009;332–337.
48. Massera JL. Contributions to stability theory. *Ann Math*. 1956;64:182–206.
49. Khalil HK. *Nonlinear Systems, 3rd ed*. Upper Saddle River, NJ: Prentice Hall, 2002.
50. Lin Y, Sontag ED. A universal formula for stabilization with bounded controls. *Syst Contr Lett*. 1991;16:393–397.

51. Kokotović P, Arcak M. Constructive nonlinear control: a historical perspective. *Automatica*. 2001;37:637–662.
52. El-Farra NH, Christofides PD. Bounded robust control of constrained multivariable nonlinear processes. *Chem Eng Sci*. 2003;58:3025–3047.
53. Christofides PD, El-Farra NH. *Control of Nonlinear and Hybrid Process Systems: Designs for Uncertainty, Constraints and Time-Delays*. Berlin, Germany: Springer-Verlag, 2005.
54. Wächter A, Biegler LT. On the implementation of an interior-point filter line-search algorithm for large-scale nonlinear programming. *Math Program*. 2006;106:25–57.
55. Alanqar A, Ellis M, Christofides PD. Economic model predictive control of nonlinear process systems using empirical models. *AIChE J*. 2015;61:816–830.
56. Muñoz de la Peña D, Christofides PD. Lyapunov-based model predictive control of nonlinear systems subject to data losses. *IEEE Trans Automat Control*. 2008;53:2076–2089.
57. Sontag ED. A 'universal' construction of Artstein's theorem on nonlinear stabilization. *Syst Contr Lett*. 1989;13:117–123.

Manuscript received May 21, 2015, and revision received June 23, 2015.